

FIELD METHODS AND PHOTOGRAMMETRIC TECHNIQUES FOR MAPPING AQUATIC VEGETATION USING UNMANNED AERIAL SYSTEMS

by

PHILIP D. ASHFORD

(Under the Direction of MARGUERITE MADDEN)

ABSTRACT

New ways to acquire aerial imagery are improving access to high-resolution aerial imagery products for research and commercial applications. While high costs have historically limited access to aerial imagery for most organizations, unmanned aerial systems (UAS) are enabling broader integration of imagery and geospatial data products to document and visualize landscapes of interest. It is more affordable than ever to acquire the necessary UAS equipment and computer software and hardware to create 3D models, digital elevation models (DEMs), and ultra-high (<10cm) resolution orthomosaic imagery. This study describes a UAS-based field survey methodology and image processing workflow used to map native, exotic and invasive aquatic vegetation. It discusses the merits and limitations of UAS for large reservoir management and ecological monitoring purposes. The results demonstrate the capacity of small UAS to survey, map, and detect features of interest over a large area and support the viability of UAS for vegetation surveying.

INDEX WORDS: unmanned aerial systems (UAS), structure from motion (SfM)
photogrammetry, environmental monitoring, reservoir management, geographic object-based
image analysis (GEOBIA)

FIELD METHODS AND PHOTOGRAMMETRIC TECHNIQUES
FOR MAPPING AQUATIC VEGETATION USING UNMANNED
AERIAL SYSTEMS

by

PHILIP D. ASHFORD

B.S.E.S., The University of Georgia, 2014

A Thesis Submitted to the Graduate Faculty of The University of Georgia in Partial Fulfillment
of the Requirements for the Degree

MASTER OF SCIENCE

ATHENS, GEORGIA

2019

© 2019

Philip D. Ashford

All Rights Reserved

FIELD METHODS AND PHOTOGRAMMETRIC TECHNIQUES FOR MAPPING AQUATIC VEGETATION USING UNMANNED AERIAL SYSTEMS

by

PHILIP D. ASHFORD

Major Professor:
Committee:

Marguerite Madden
Stephen Golladay
Deepak Mishra

Electronic Version Approved:

Ron Walcott
Interim Dean of the Graduate School
The University of Georgia
December 2019

DEDICATION

This work is dedicated to Louisa. If you ever stumble across this in the library repository during your own academic career, which is sure to surpass my own, know that you were always a welcome distraction.

ACKNOWLEDGEMENTS

I would like to express my appreciation to my major professor, Dr. Madden, as well as my reading committee, Drs. Golladay and Mishra. Thank you all for your support, assistance, and patience throughout this process.

I would also like to thank the Jones Center at Ichauway and the Graduate School of the University of Georgia for the funding that make this research possible.

Many thanks to Jody Timmons at the USACE Lake Seminole Field office for facilitating the permitting process without which this study would not have been possible, and to Brent Mortimer, USACE Aquatics Specialist, for giving me a tour of the reservoir and sharing his extensive knowledge of the aquatic plants therein.

TABLE OF CONTENTS

	Page
ACKNOWLEDGEMENTS.....	v
LIST OF FIGURES	viii
LIST OF TABLES	x
CHAPTER	
1 Introduction	1
Background	1
Remote Sensing Assessment of Nuisance Aquatic Vegetation	3
Study Area.....	5
Research Objectives	13
2 Review of Concepts and Literature	14
Aquatic Ecology	14
Remote Sensing	17
3 Methodology	21
Small Unmanned Aerial Systems (sUAS) Regulatory Environment.....	22
Site Considerations	24
Survey Equipment.....	27
Survey Design.....	29
Data Acquisition	33
Photogrammetric Processing	37
Geographic Object-Based Image Analysis (GEOBIA).....	45

4	Results	50
5	Discussion and Conclusion	60
	Limitations.....	60
	Future Directions	64
	Conclusion.....	66
	REFERENCES	68

LIST OF FIGURES

	Page
Figure 1.1: Map of Lake Seminole, Georgia study area.....	5
Figure 1.2 (a-c): Common vegetation assemblages in Lake Seminole: (a) floating-leaf dominant, (b) hydrilla dominant, and (c) macrophyte and floating leaf mix.....	8
Figure 1.3: Common aquatic vegetation species found in Lake Seminole, photographed from ground-level (left) and the corresponding aerial view (right), including: a) American Lotus (<i>Nelumbo lutea</i>); b) Hydrilla (<i>Hydrilla verticillata</i>); c) Pondweed (<i>Elodea canadensis</i>); d) Cuban Bulrush (<i>Oxycaryum cubense</i>); e) Waterlily (<i>Nymphaea</i>); f) Water Hyacinth (<i>Eichhornia</i> <i>crassipes</i>); g) (<i>Lyngbya wollei</i>); and h) Muskgrass (<i>Chara</i>)	10
Figure 3.1: Conceptual diagram of survey design for UAS data acquisition	21
Figure 3.2: UAS coverage of study area by survey year.....	25
Figure 3.3: Photograph of field survey equipment and operating conditions.....	29
Figure 3.4: Striping in an orthomosaic from cloud-induced overexposure.....	31
Figure 3.5: Examples of flight line and sensor orientations used: a) a problematic flight design; and b) an optimal flight design	32
Figure 3.6: Diagram of the photogrammetric reconstruction workflow used.....	44
Figure 3.7: The impact of minimum segment size on segmentation results, showing minimum segment sizes, from left to right, of: 1, 16, and 1600	46
Figure 4.1: UAS orthomosaic coverage of Lake Seminole in 2016	52
Figure 4.2: Unsupervised ISO classification of vegetation in Lake Seminole	52
Figure 4.3: Map of Sealy's Point vegetation classification test area	53

Figure 4.4: Map displaying the results of an in-situ vegetation survey of Sealy’s Point performed by Shivers in 2014.....	53
Figure 4.5 (a-b): UAS orthomosaic image (a) and segmented raster (b) of Sealy’s Point study area.....	54
Figure 4.6 (a-d): Supervised and unsupervised classification results of Sealy’s Point study area using (a) Maximum Likelihood (b) ISO Cluster (c) Random Forest and (d) Support Vector Machine Classifiers.....	55

LIST OF TABLES

	Page
Table 1: Species of Aquatic Vegetation Present in Lake Seminole.....	9
Table 2: Summary Statistics for UAS Surveys of Lake Seminole by Survey Year.....	24
Table 3: Vegetation Classification Scheme	48
Table 4: Confusion Matrices for (a) Maximum Likelihood Classifier, (b) ISO Cluster Classifier, (c) Random Trees Classifier, and (d) Support Vector Machine Classifier	57

Chapter 1

Introduction

Background

Until recently and despite great potential, unmanned aerial systems (UAS) were not broadly integrated into resource management, academic research and commercial activities in the United States due to a number of regulatory, social, and technical factors. Prior to the establishment of the Small UAS Rule, 14 CFR Part 107 (Part 107) in September 2016, the Federal Aviation Administration (FAA) maintained a proscriptive regulatory environment regarding commercial UAS operations while it developed the procedures and infrastructural capacity to implement a nationwide Unmanned Aircraft Traffic Management System (UTM). The goal of the UTM is to safely integrate UAS into the National Airspace System (NAS), allowing commercial UAS operations while giving air traffic controllers positional awareness of and a method to communicate with UAS, thus minimizing the potential for mid-air collisions with other manned and unmanned air traffic. An additional concern is preventing the unauthorized incursion of UAS into restricted airspace or sensitive national security areas (USDOT 2013).

Substantial public opposition to commercial UAS operations in the NAS is attributable in part to the conflation of UAS with military action by news and entertainment outlets, and fears that fundamental notions of property and privacy rights are imperiled by the abuse or misuse of aerial surveillance by domestic law enforcement agencies or unscrupulous individuals. Some commercial uses have also raised the specter of nuisance and noise pollution, in particular the

use of unmanned aircraft for the transportation of property for compensation or hire (McNeal 2014). FAA's approval of some commercial UAS operations under Part 107, as well as the recent growth in popularity of small UAS for recreational use have made them a common sight, which has helped to diminish public opposition.

Over the last decade, advances in UAS technology in terms of their affordability, ease of operation, flight duration, and sensor quality have made them a viable alternative to manned aircraft for a number of aerial imaging applications. The revolutionary capabilities of UAS are empowering researchers and resource managers with an efficient means to conduct ecological monitoring using unmanned aerial surveys, particularly for environments that are difficult to access from the ground or to visualize using higher-altitude remote sensing platforms. The ultra-high spatial resolution and image quality from low-altitude acquisition of UAS imagery outperforms the best-available commercial satellite imagery, and is less expensive to acquire, particularly for multi-temporal data.

UAS also offer economic advantages compared to manned aerial photography. When compared to manned aircraft, UAS are much less expensive to own and operate in terms of acquisition, maintenance, fuel, and the cost to obtain pilot licensure. Low altitude flight obviates the need for post-processing to correct for the effects of atmospheric distortion and enables operation under cloudy conditions. First-person view (FPV) video transmission allows UAS operators to view collected imagery in near real-time and adjust the flight path and sensor orientation as needed, making UAS much more responsive to atmospheric conditions or terrain characteristics than manned aircraft (Hardin et al. 2019). In aquatic environments, this versatility can minimize the adverse impact of specular reflectance, also referred to as sun glint, allowing more reliable visualization of submerged features.

In recent years, UAS imagery has been used in numerous government and commercial applications and academic disciplines, including disaster management and emergency response (Antonio 2016), architecture and construction (Levin et al. 2017), agriculture (Hassler and Baysal-Gurel 2019), archaeology (Waagen 2019, Wang et al. 2019), and journalism (Adams 2019). Similarly, UAS is proving to be a valuable tool, offering researchers and resource managers a potentially unprecedented capacity to remotely observe and analyze ecological phenomena and processes (Tamminga et al. 2015). Indeed, the revolutionary power of UAS for resources management lies in the ability to tailor the spatial extent, resolution, and temporal frequency of the data to suit specific research objectives (Madden et al. 2015 and 2019). This study assesses the overall feasibility of a UAS-based survey approach as compared to traditional field and remote sensing methods. It also provides a description of UAS operations in challenging field conditions and identifies a set of computational resources and techniques to photogrammetrically process large data volumes and create detailed digital image products for aquatic resource research, assessment, and management.

Remote Sensing Assessment of Nuisance Aquatic Vegetation

Nuisance aquatic vegetation has become a global environmental issue associated with landscape development, eutrophication of waterways, and climate change (Shivers et al. 2018a and 2018b). Aquatic vegetation occurs naturally in creeks, rivers, ponds, lakes and coastal ocean water bodies, given proper substrate, nutrients and sunlight. Water quality, quantity and clarity can determine the types, abundance and distribution of plants within aquatic systems. A diversity of aquatic plant species may include plants that are free floating on the water surface, rooted in the substrate with leaves floating on the surface, rooted and emerging above the surface and/or

rooted growing submergent or below the surface (Fassett and Ogden 1957, Magee 1981, Aulbach-Smith and deKozlowski 1990). Resource managers are often concerned with aquatic vegetation inventory and monitoring (Remillard and Welch 1992 and 1993), especially the displacement of naturally diverse aquatic plant communities by monotypic stands of native and exotic invasive species. Lake managers require efficient methods of detecting invasive plants, mapping their distributions, monitoring their spread and determining the effectiveness of management decisions (Bogucki et al. 1980, Madden 2004).

Remote sensing has been used for decades to map the seasonal growth and distribution of aquatic vegetation and particularly, submerged aquatic vegetation (SAV), using imagery collected by manned aircraft (Schneider 1966 and 1968, Gammon and Carter 1979, Bogucki et al. 1980, Welch et al. 1988 and 1992) and satellites (Carter and Schubert 1974, Butera 1983, Jensen et al. 1984, 1986 and 1987). While these methods are often capable of detecting the presence of SAV, widespread adoption of remote sensing methods for aquatic vegetation monitoring has been constrained by the high cost and limited ability to detect submerged features under all but ideal hydrologic and atmospheric observing conditions (Remillard and Welch 1992 and 1993). This study evaluates the use of UAS imagery in monitoring the seasonal growth and spatial extent of submerged, emergent and free-floating aquatic vegetation in Lake Seminole, a large subtropical reservoir located in Southwest Georgia. Lake Seminole has a history of nuisance vegetation assessment and considerable investment in control efforts. As such, it is well suited to testing the utility of UAS-based remote sensing techniques and analysis.

Study Area

The Apalachicola, Chattahoochee, and Flint Rivers and their respective watersheds cover more than 52,000 km² across three states and are collectively referred to as the Apalachicola-Chattahoochee-Flint (ACF) Basin (see inset map of Figure 1.1). This Basin contains diverse aquatic resources that support important regional economic and recreational uses including power generation, municipal water, agricultural irrigation, boating and fishing (Frick et al.1998).

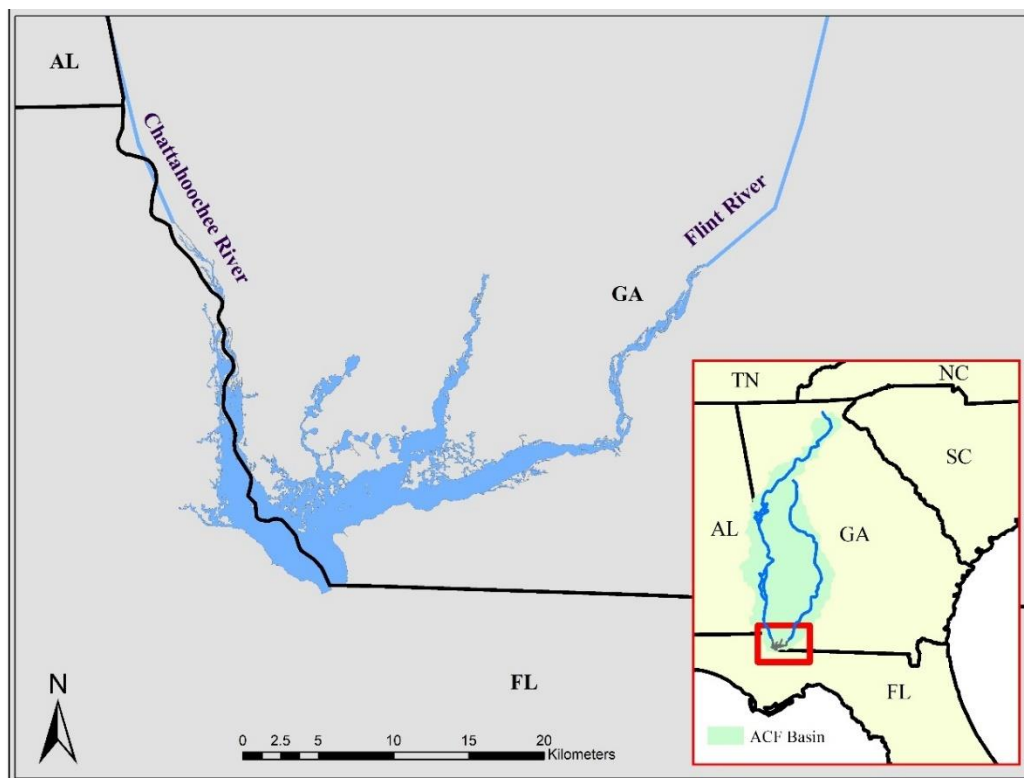


Figure 1.1: Map of Lake Seminole, Georgia study area

Conflicting priorities between the states of Alabama, Florida, and Georgia regarding issues related to the use and management of the ACF River Basin have resulted in a series of lawsuits, counter-suits, and appeals which ultimately reached the United States Supreme Court, where the case is currently being arbitrated by a Court-appointed Special Master (Hallerman 2018). The legal fracas has been so protracted and divisive that it has become known as the “Tri-State Water

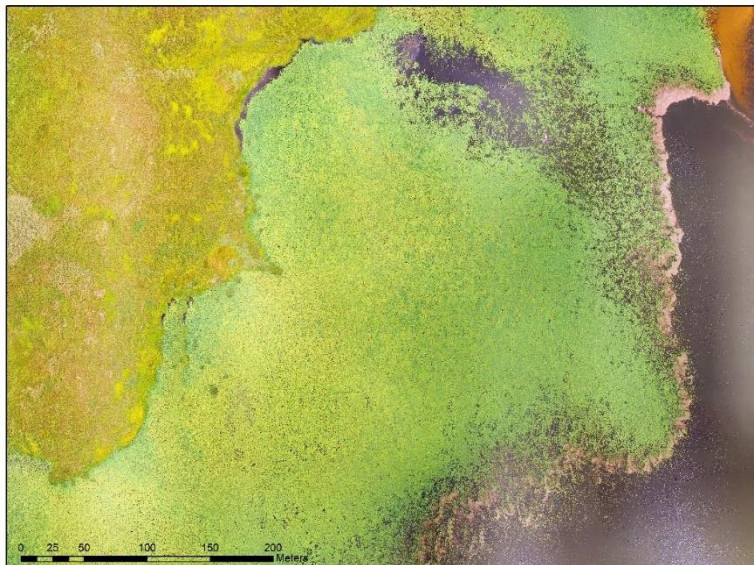
Wars”. One of the central issues is the contention made by Florida that Georgia’s ground- and surface water withdrawals from the ACF Basin for municipal and agricultural use have an adverse effect on water quality in the Apalachicola River, and that reduced flows attributable to excessive upstream usage pose a threat to environmentally-sensitive and commercially-important fisheries (ARC 2018a and 2018b). Lake Seminole, located partly in Georgia (Decatur and Seminole Counties) and Florida (Gadsden and Jackson Counties), is a large, shallow, run-of-the-river reservoir located where the Chattahoochee and Flint Rivers meet to form the Apalachicola River. As the nexus of the ACF River system, Lake Seminole exhibits a complex and varied ecology which impacts downstream water quality and make it a relevant and multifaceted object of study. Biogeochemical processes within the reservoir are greatly affected by the annual growth and relative composition of a number of species of aquatic vegetation, in particular the non-native and submergent aquatic macrophyte, *Hydrilla verticillata* (Shivers 2018a). Lake Seminole encompasses diverse physical, chemical, and hydrologic conditions, which affect patterns and assemblages of vegetation growth. This results in a marked difference in the composition of plant communities within Lake Seminole, particularly between the Chattahoochee arm and Flint/Spring Creek arms of the reservoir. The growing conditions for aquatic vegetation in each arm of the reservoir are largely determined by the characteristics of their tributaries, which are in turn determined by the soil characteristics and pattern of land use of their respective watersheds. The Chattahoochee and Flint rivers are strikingly different. The Chattahoochee River is the most regulated river in Georgia with 13 dams, receives effluent from 120 publicly-operated treatment works (POTWs) including Atlanta and Columbus, and has comparatively little agricultural runoff. The Flint River is predominantly free-flowing, receives effluent from only 60 smaller POTWs, and receives large amounts of agricultural runoff (Frick et

al. 1998). Due to these factors, the Chattahoochee arm is less turbid, experiences fewer and less severe fluctuations in water level, and has lower N and P concentrations than the Flint arm (Waters et al. 2015). The coexistence of two hydrologic regimes within the same water body is reflected in the assemblages of aquatic vegetation present. In the Chattahoochee arm, floating leaf vegetation, including water hyacinth, waterlily, lotus, and watershield predominates, while the Flint and Spring Creek arms are macrophyte-dominant (Shivers et al. 2018a). The macrophytes present in Lake Seminole include hydrilla, pondweed, eurasian watermilfoil, coontail, limnophila, cabomba, and fanwort. Muskgrass, a freshwater green alga, is non-vascular but assumes the appearance of a macrophyte in its growth form and predominates in some areas, particularly in the middle of dense macrophyte beds where there is lower nutrient and oxygen availability (Partridge 1996). Lyngbya, a cyanobacteria which forms dense mats of fibrous material on the reservoir's surface, can periodically engulf other aquatic vegetation in the reservoir at certain times of year, particularly at the end of the growing season or following the application of aquatic herbicides. In a nutrient-rich environment such as Lake Seminole, cyanobacteria proliferation tends to occur in the absence of competition for those nutrients by aquatic vegetation (NASA DEVELOP 2014). Cyanobacteria are of particular concern to resource managers since they extrude compounds whose toxicity can range from a mild skin irritant to potent neuro- and hepatotoxins. Lyngbya has adversely affected wildlife (Dodd et al. 2016), and poses a risk to humans as well. Its prevalence in Lake Seminole and its potential for adverse health impacts justified including lyngbya in the vegetation map in this study. However, because the appearance of lyngbya in the imagery was the same as senescent macrophytes, it was ultimately combined with the mixed macrophyte class. Riparian grasses, including Cuban bulrush and giant cutgrass, are present throughout the reservoir along the shoreline. Giant

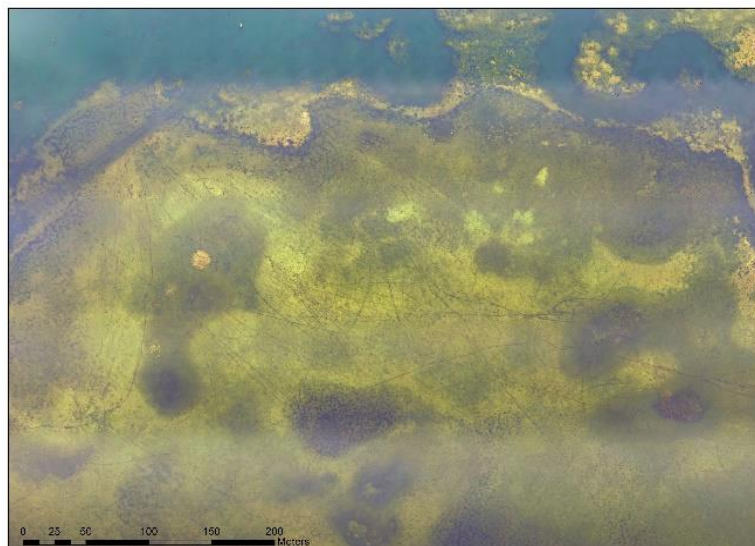
cutgrass's dense growth form and expansive inter-annual growth (Fox and Haller 2000) caused difficulty in determining the apparent shoreline between years and obscured the precise border between land and water in the imagery.

Figure 1.2 depicts the range of vegetative assemblages in Lake Seminole, including (a) floating-leaf dominant, (b) hydrilla dominant, and (c) mixed aquatic vegetation. Table 1 lists the primary aquatic species found in the reservoir. Figure 1.3 displays an aerial and terrestrial view of the most commonly observed and identifiable species in the survey.

(a)



(b)



(c)

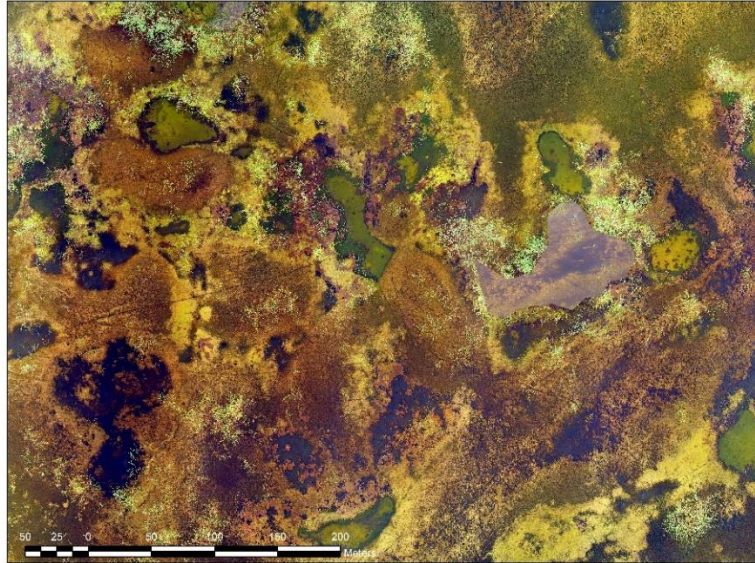





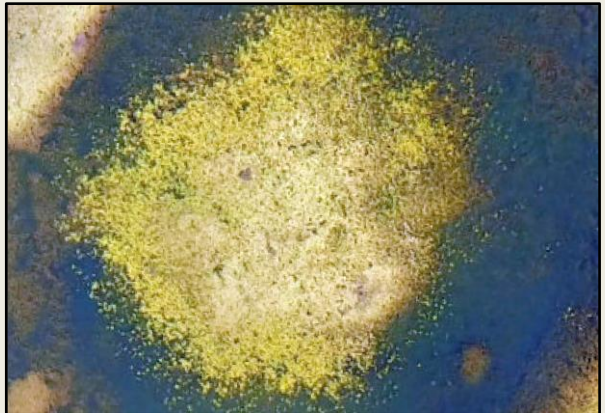


Figure 1.2: Common vegetative assemblages in Lake Seminole: (a) Floating-leaf dominant, (b) Hydrilla dominant, and (c) Macrophyte and floating leaf mix

I – SUBMERGED AQUATIC VEGETATION (SAV)	III – FLOATING LEAF
1.1 <i>Hydrilla verticillata</i> (Hydrilla)	3.1 <i>Eichhornia crassipes</i> (Water Hyacinth)
1.2 <i>Elodea canadensis</i> (Pondweed)	3.2 <i>Nymphaea</i> spp. (Waterlily)
1.3 <i>Limnophila sessiflor</i> (Limnophila)	3.3 <i>Nelumbo lutea</i> (American Lotus)
1.4 <i>Myriophyllum spicatum</i> (Eurasian water-milfoil)	3.4 <i>Brasenia schreberi</i> (Watershield)
1.5 <i>Cabomba caroliniana</i> (Fanwort)	IV – RIPARIAN
1.6 <i>Ceratophyllum demersum</i> (Coontail)	4.1 <i>Zizaniopsis miliacea</i> (Giant Cutgrass)
1.7 <i>Chara</i> (Muskgrass, Stonewort)	4.2 <i>Phragmites australis</i> (Phragmites)
II – OPEN WATER	4.3 <i>Oxycaryum cubense</i> (Cuban Bulrush)

Table 1: Species of Aquatic Vegetation Present in Lake Seminole (Brent Mortimer, USACE

Aquatics Specialist, personal communication)

Ground View	Aerial View
 <p>a)</p>	
 <p>b)</p>	
 <p>c)</p>	



d)



e)



f)



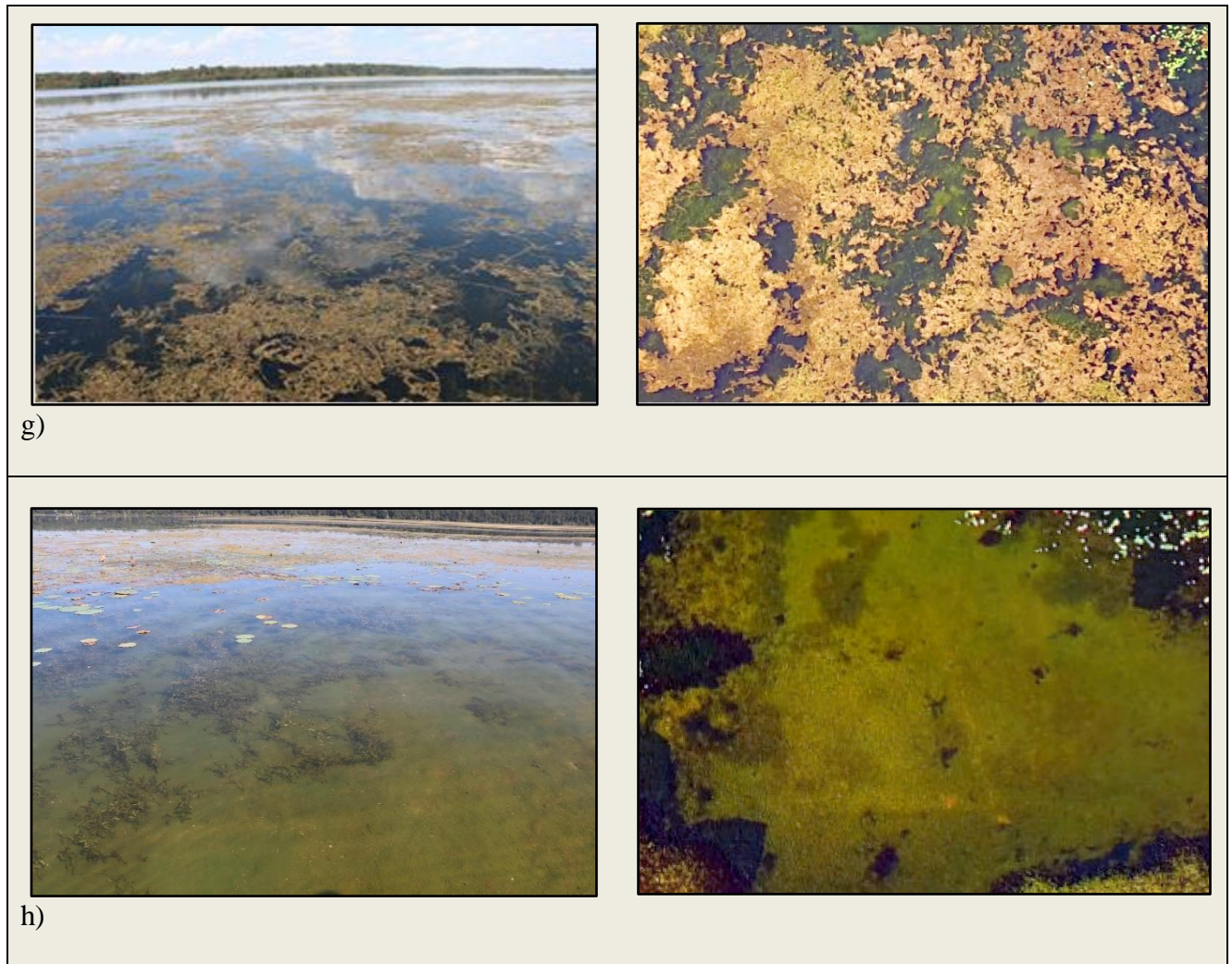


Figure 1.3: Common aquatic vegetation species found in Lake Seminole, photographed from ground-level (left) and the corresponding aerial view (right), including: a) American Lotus (*Nelumbo lutea*); b) Hydrilla (*Hydrilla verticillata*); c) Pondweed (*Elodea canadensis*); d) Cuban Bulrush (*Oxycaryum cubense*); e) Waterlily (*Nymphaea*); f) Water Hyacinth (*Eichhornia crassipes*); g) (*Lyngbya wollei*); and h) Muskgrass (*Chara*)

Research Objectives

Given the impact of aquatic vegetation in Lake Seminole on ecological processes that affect water quality and quantity (Partridge 1996), this study aims to develop a methodology that can be used to effectively assess the abundance and distribution of aquatic vegetation species at a high level of spatial and temporal resolution. The method should be relatively cost efficient, use readily available equipment and software, include a defined and tested workflow for data collection, processing and analysis, and provide researchers and resource managers with information required for both understanding the complex aquatic system and making sound management decisions.

Specific objectives are:

1. To develop a methodology using Unmanned Aerial System (UAS) technology to acquire true-color aerial imagery of a large reservoir at multiple time periods, use best practices for the management of large image data sets and perform Structure from Motion photogrammetry to create fine-scale digital elevation models and seamless orthomosaics suitable for mapping and monitoring aquatic vegetation;
2. To use these image data to classify and map emergent, submerged, and free-floating aquatic vegetation, with particular emphasis on *H. verticillata* (hydrilla); and
3. Determine whether UAS imagery can be applied to detect inter- and intra-annual changes in vegetation coverage

Chapter 2

Review of Concepts and Literature

This chapter summarizes the literature and concepts which contribute to the theoretical framework of this study and highlight the progression of remote sensing applications to vegetation mapping and aquatic ecosystems monitoring.

Aquatic Ecology

As in many reservoirs throughout the Southeastern United States, *Hydrilla verticillata*, commonly known as hydrilla, has been the predominant form of aquatic vegetation in Lake Seminole since shortly after its accidental introduction to the reservoir in the 1960's (Eubanks and Morgan 2001). A submergent macrophyte native to subtropical Southeast Asia, hydrilla thrives in Lake Seminole's warm, shallow waters with low turbidity and high nutrient content. Hydrilla growth provides numerous beneficial ecosystem services, enhancing water quality through phytoremediation, the uptake of harmful substances into the plant's biomass (Chathuranga et al. 2014, Shivers et al. 2018), nutrient sequestration (Wang et al. 2007), inhibition of harmful algal growth (Zhang et al. 2012), and providing habitat for aquatic organisms (Sammons and Maceina 2006). Conversely, due to its invasiveness and potential for explosive growth which can outcompete other forms of submerged aquatic vegetation and reduce overall species diversity (Cox et al. 2014), hydrilla is classified as a noxious weed in most areas of the United States (Evans et al. 2005).

Hydrilla grows into dense, extensive beds which span the depth of the water column in the photic zone and represent a serious navigation hazard, as plant material can easily become entangled in

conventional outboard boat motors, stalling or even destroying them. The United States Army Corps of Engineers (USACE), vested with the responsibility to manage all navigable waterways in the United States, has employed numerous methods in its attempt to control or eradicate hydrilla. Control measures include manual removal, chemical and biological controls, manipulating environmental parameters known to affect hydrilla growth, and developing predictive models to simulate hydrilla response to the other control techniques (Welch et al. 1988, Kumar et al. 2019). One of the most effective means to control hydrilla has been the application of the aquatic herbicide fluridone. However, even if herbicides are used to treat the foliage, hydrilla can regenerate from its turions, tubers submerged in the sediments. Prolonged aquatic herbicide use also leads to the proliferation of herbicide-resistant genetic variants of hydrilla. For example, in Florida's Kissimmee Chain of Lakes a fluridone-resistant strain of hydrilla persists as the dominant phenotype even eight years following the cessation of fluridone applications (Netherland and Jones 2015). As with any systemic herbicide application, there is a potential for unintended adverse effects on plants and animals other than the target species. Freshwater mollusks are just one species experiencing collateral damage from chemical hydrilla control regimes (Archambault et al. 2015).

While in some areas USACE efforts have achieved localized elimination of or a reduction in hydrilla coverage, eradication remains an elusive goal (Cox et al. 2014). For the foreseeable future, hydrilla will continue to dominate the assemblage of aquatic vegetation found in Lake Seminole and in shallow reservoirs throughout subtropical regions of the United States. With dismal prospects for complete eradication, scholarship and reservoir management are transitioning towards more targeted, local intervention and the development of long-term monitoring strategies using ground-based and remote sensing technologies to: (1) detect and map

hydrilla coverage; (2) better understand the environmental and climatic factors that influence its growth and distribution; and (3) examine its role in influencing aquatic ecological and biogeochemical processes (Remillard and Welch 1992, Rotta et al. 2016, Kumar et al. 2019). To that end, researchers at the Joseph W. Jones Ecological Research Center have for the last several years conducted surveys documenting the intra- and inter-annual changes in the spatial extent and species composition of Lake Seminole's aquatic vegetation (Shivers et al. 2018a and 2018b, NASA DEVELOP 2014). A number of survey methods have been employed, including boat-based global positioning system (GPS) data collection and remote sensing approaches. GPS-based field surveys of the reservoir have been conducted to determine the maximum spatial extent of hydrilla and relate its growth to environmental factors such as turbidity and nutrient availability. Shivers et al. (2018a) provided GPS-based vegetation coverage estimates for the reservoir over a three-year period. The survey was limited to peak coverage, late August and September, and took two people, a GPS unit, and a specialized boat four to six weeks to complete, plus substantial post processing. They observed annual variation in SAV coverage which was linked to water clarity associated with flood pulses during the growing season. However, a limitation (other than time and cost) was only semi-quantitative estimates of SAV bed composition. Additionally, a 2014 NASA DEVELOP project used Lake Seminole as a study area and compared 30-meter resolution Landsat imagery with in-situ data reflectance data in an effort to detect and map seasonal hydrilla growth (NASA DEVELOP 2014). This study was limited by rather coarse spatial resolution (30m) of the Landsat-8 Operational Land Imager (OLI) sensor imagery, as well as frequent cloud cover in the region during the growing season.

Remote Sensing

A consistent feature in the development of the remote sensing field is that the emergence of novel means to acquire data precipitates advances in related technologies, techniques and best practices that are better able to exploit the new data. Remote sensing has been used for decades to map the seasonal growth and distribution of submerged aquatic vegetation (SAV) using imagery collected by satellites and manned aircraft (Welch et al. 1988, Schuchman et al. 2013, Fritz et al. 2017), but it has only very recently become possible to conduct such studies using UAS (Colomina and Molina 2014, Mishra et al. 2018). In the United States, the ban on commercial UAS operations prior to promulgation of Part 107 largely precluded academic and educational use, limiting the overall contribution of American universities and research institutions to the literature of applied UAS studies.

Since the mid-2010s, the rapidly improving capabilities and relative affordability of UAS have been leveraged for mapping aquatic environments. Flynn and Chapra (2014) used a quadcopter UAS to acquire aerial images of the Clarke Ford River in western Montana at 18 time periods during the growing season in order to map the seasonal development of the nuisance algae *Cladophora glomerata*. Feature detection was then applied to the orthomosaic imagery to delineate the percentage of the study area affected by *Cladophora* at each time interval. They report 90-92% accuracy in identifying *Cladophora*, but did not map any other species of aquatic vegetation. Flynn and Chapra (2014) focused only on identifying a single species, and the accuracy values would likely be lower in the event that other algae or aquatic vegetation were present.

Tung-Ching and Chou (2015) used a fixed-wing UAS to map aquatic vegetation in a small reservoir in Taiwan and relate vegetation coverage to water quality parameters from in-situ water

sampling. UAS was shown to fill spatiotemporal gaps in available satellite data that would otherwise confound mapping of highly localized, seasonal events such as aquatic vegetation growth. Without the high spatiotemporal resolution offered by the UAS, it was not possible to link vegetation growth with other water quality parameters using regression modeling. Their study linked UAS imagery with simultaneously collected water quality information (turbidity, in situ nutrient and phytoplankton measurements). The UAS sensor was modified to record green, red, and near-infrared (NIR) spectral bands to create false color composite images. With ground control points, the final model achieved a spatial accuracy of $\pm 4.5\text{cm}$. The final results were used to develop a regression model predicting chlorophyll-a and total phosphorus concentrations, with highly significant results ($P < 0.05$, $r^2 > 0.9$).

Very high spatial resolution imagery has been used to differentiate between and classify surface features and various species of vegetation in aquatic ecosystems using geographic object-based image analysis (GEOBIA) process (Hay and Castilla 2008). GEOBIA consists of image segmentation, training area selection and feature classification, and may either be an automated (unsupervised) or semi-automated (supervised) process (Hay et al. 2002, Lang et al. 2009, Blaschke et al. 2014). During image segmentation, statistical measures of the spatial relationship and spectral similarity between adjacent pixels are used to partition a raster image into pixel groupings representing discrete image objects (Blaschke et al. 2008). The segmentation process can yield segments of a range of sizes by altering the input parameters, which include scale factor, merge factor and kernel size. The scale parameter determines the number of iterations in the algorithm and ultimately controls the size of the output image-objects. As the scale parameter increases, there are fewer iterations and the pixel groupings are coarser. For unsupervised classification, the user simply specifies a target number of classes, and segments are grouped into

the specified number of classes automatically using an unsupervised classification algorithm such as ISODATA or Maximum Likelihood Classifier (MLC) (Green 2017). For a supervised classification, training area selection must be conducted manually. Training area selection involves identifying portions of the segmented raster which represent a particular feature or land cover type (Green 2017). Training area samples should reflect the range of spectral and textural heterogeneity that exist within a particular class across the study area. In situations where excessive in-class spectral variation exists due to differences in phenology or illumination, certain features may have to be split into more than one class during training area selection and merged following the classification step. The training areas identified are used as input to classify the remainder of the segmented raster, using a machine-learning algorithm such as support-vector machine (SVM) or random forest/random trees (Blascke 2010).

Kim et al. (2011) compared the classification accuracy of single-scale and multi-scale GEOBIA and the effect of incorporating ancillary data to map water, vegetation, and bare mud in a salt marsh ecosystem. Segmentation was achieved using the Multiresolution Segmentation (MRS) algorithm, which computes spectral and shape heterogeneity of neighboring pixels and groups them according to the scale parameter. They reported user's accuracy of 82% for their most detailed model.

Zhang et al. (2013) used a method called ensemble analysis to incorporate multiple separate datasets with varying spatial resolution as part of a GEOBIA classification to map vegetation in the Florida Everglades. The combination of Light Detection and Ranging (LiDAR) elevation data, multispectral satellite imagery, and true-color National Agricultural Imagery Program (NAIP) imagery produced a highly accurate (91%) map of 11 vegetation types. While it did not utilize UAS imagery, this study demonstrates how elevation data can be incorporated as ancillary

data in an image classification workflow to improve feature detection and presents a possible method for enhancing true-color UAS imagery with multispectral information from satellites. This study will contribute to the literature on UAS-based remote sensing of aquatic vegetation by identifying best practices and operational limitations for UAS operations in subtropical environments. The literature review indicates that there is a much greater focus on data processing and image analysis than there is on data acquisition. This study will also address questions of scale. By attempting to map such a large extent ($\sim 90\text{km}^2$), the feasibility of implementing UAS in favor of alternative remote sensing platforms for monitoring at a landscape scale will be assessed.

Chapter 3

Methodology

This chapter provides an overview of the factors which influenced survey design and implementation (Figure 3.1), and methods used to preprocess, photogrammetrically-reconstruct, and classify the aquatic vegetation survey data.

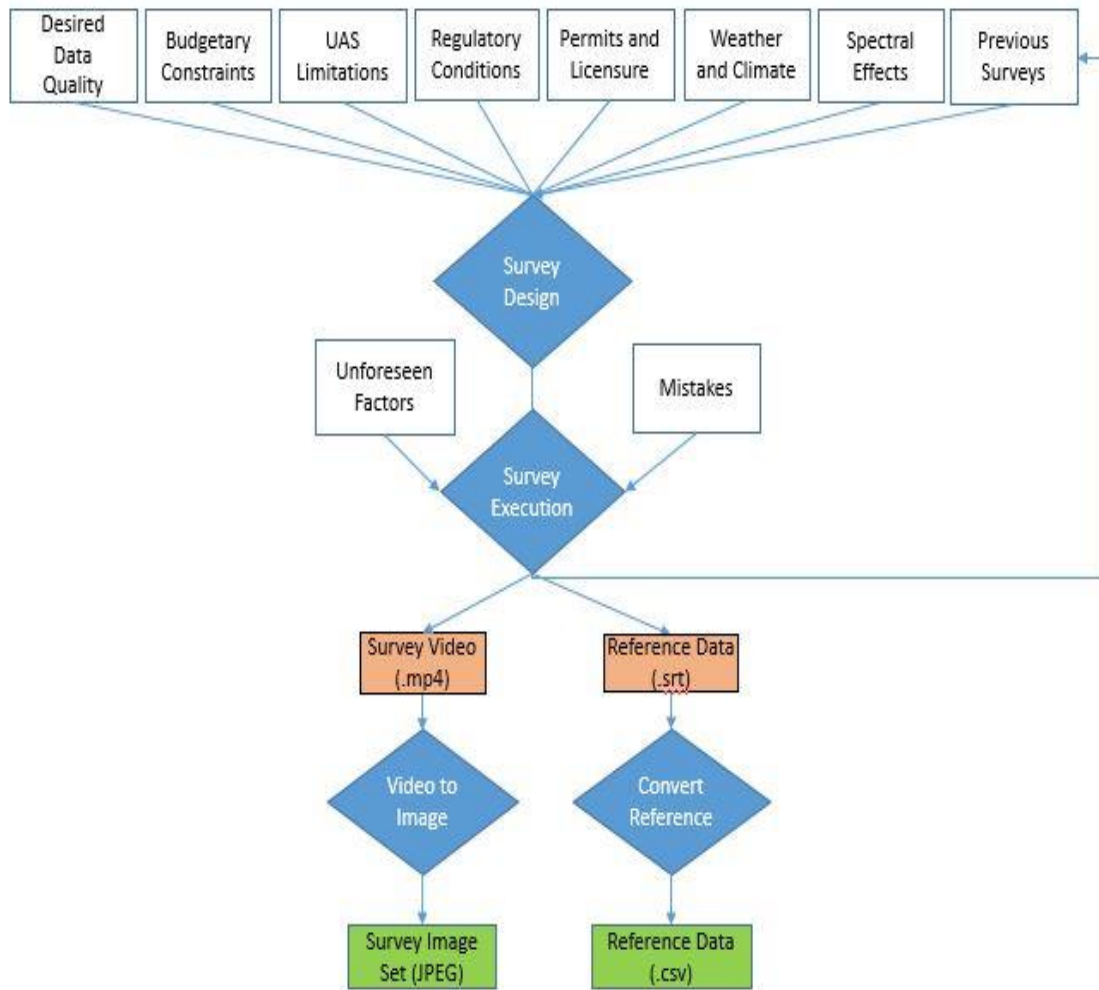


Figure 3.1: Conceptual Diagram of Survey Design for UAS Data Acquisition

Small Unmanned Aerial Systems (sUAS) Regulatory Environment

Prior to the Small UAS Rule taking effect in 2016, it would have required a manned pilot's license to conduct the survey described herein for commercial, research, or educational purposes under the auspices of any private corporation, nonprofit, or academic institution. Only recreational use was permitted under Part 101(e). The only legal means of procuring permission to operate a UAS commercially was a Section 333 exemption. Section 333 exemptions were awarded sparingly and at the FAA's sole discretion. The application process was lengthy and expensive and there was no guarantee that the request would even be considered. Part 107, issued in August of 2016, was widely lauded for establishing a clear set of rules for remote pilot licensure and defining operating conditions of small unmanned aircraft systems (sUAS) (FAA 2016).

To become certified as a remote pilot under Part 107, the applicant must be a US citizen, clear a background check and pass an aeronautical knowledge exam every two years. Commercial UAS operations are limited to under 400 feet (121.9 meters) above ground-level (AGL) during daylight hours in Class G airspace, with flights in Class D and E airspaces allowable subject to approval by local air traffic control. UAS operations are precluded in all restricted areas that are published in aeronautical charts or announced through FAA's Notice to Airmen (NOTAM) system. Laws, ordinances, and regulations at the local, state, or federal level may exclude additional areas or add other operating restrictions. Since this study proposed operating over a reservoir managed by USACE, it was necessary to obtain a Special Activities Permit from the USACE district office in Mobile, Alabama. As a condition of the permit, operations were required to maintain a minimum distance of 150 meters away from three security-sensitive sites: the USACE Lake Seminole field office, the Woodruff Lock and Dam and hydro-electric power

plant, and a correctional facility in Sneads, Florida. Prudence suggested maintaining a more generous buffer. These three facilities are collocated at the southernmost extremity of the reservoir, which is where the reservoir is deepest. Although hydrilla and other aquatic plant species are present to some extent in this area, they are limited to near-shore verges and are insignificant when compared to the vast vegetated expanses covering much of the rest of the reservoir. As such, it was reasoned that this area could be omitted without harming the ability to accurately estimate vegetation coverage for the reservoir as a whole. If necessary, vegetative coverage in these areas could be estimated using conventional survey methods, or by assuming based on bathymetric data that aquatic vegetation is present at water depths less than three meters.

Further operational conditions under Part 107 are that the UAS must weigh less than 55lbs (<25kg), not exceed 160 kilometers-per-hour, and the remote pilot must keep the UAS within either their visual line of sight or that of a designated visual observer with whom they are in direct communication. The UAS cannot be operated directly over non-participating individuals or from a moving vehicle, except in unpopulated or very remote areas. The remote pilot assumes responsibility for ensuring that the UAS is in good condition and must maintain it or make repairs as recommended by the manufacturer. Any UAS operation which does not meet these requirements must receive a waiver from the FAA prior to execution, for which the applicant must demonstrate that sufficient risk mitigation for the proposed operations are in place.

This survey complied with all the above listed requirements, including UAS registration, remote pilot certification, the receipt additional airspace authorization, and rules for commercial operations under Part 107.

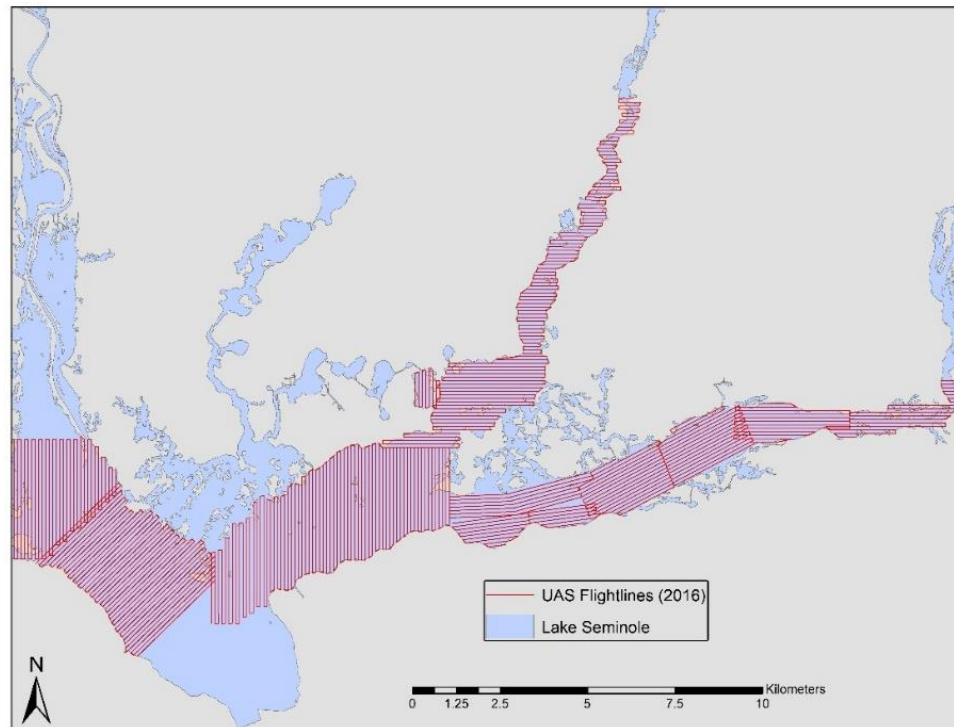
Site Considerations

In 2016, the area surveyed consisted of the entire reservoir, with the exception of some backwater areas, riverine portions of the Flint River and Chattahoochee arms of the reservoir, and areas where UAS operations were not allowed per the conditions of the special activities permit. In 2017, after a review of the 2016 survey, it was decided to omit certain areas of the reservoir whose bathymetric depth or other hydrologic factors made the presence of aquatic vegetation unlikely. Figure 3.2 provides a depiction of the areas surveyed in 2016 (Figure 3.2 (a)) and 2017 (Figure 3.2 (b)). Table 2 summarizes the individual and aggregate geographic extent of the surveys, and the associated data volumes.

	2016	2017	Total
Data Volume: Video (GB)	618.6	302.4	921.0
Data Volume: Image (GB)	351.0	169.2	520.2
Data Volume: Orthomosaic (GB)	20.2	28.0	48.2
Data Volume: Total (GB)	989.8	499.6	1,489.2
Flight Line Distance (km)	736.37	769.93	1,506.30
Reservoir Area (km ²)	116.37	116.37	116.37
Total Area Video Coverage (km ²)	77.06	78.30	155.36
Reservoir Area Video Coverage (km ²)	66.77	61.83	128.60 (gross) 88.27 (net)
Reservoir Area Orthomosaic Coverage (km ²)	38.75	29.42	49.02
Data Reconstructed (%)	58.0%	47.6%	55.5%
Reservoir Area Reconstructed (%)	33.3%	25.3%	42.3%

Table 2: Summary statistics for UAS surveys of Lake Seminole by survey year

(a)



(b)

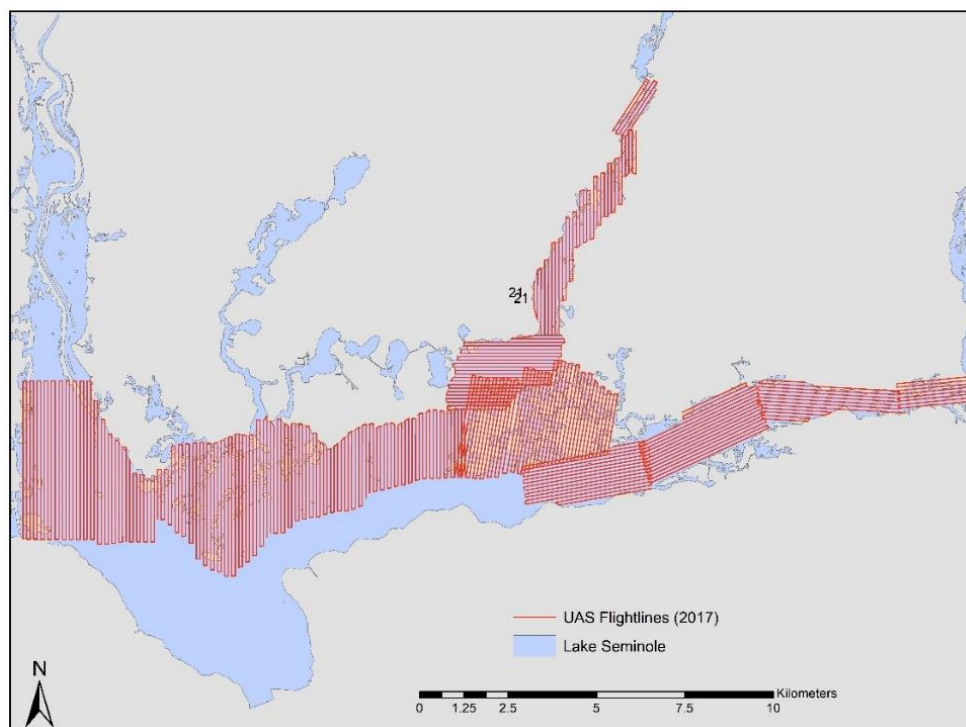


Figure 3.2: UAS coverage of study area in survey years 2016 (a) and 2017 (b)

The nature of the land use surrounding the reservoir was also taken into consideration during flight planning. Lake Seminole has a number of residential developments along the shore, as well as a great deal of State-owned timber land and protected wildlife refuges. Survey flight plans were designed to avoid encroachment on private property and minimize the potential for nuisance, as UAS operations near one's back yard or boat dock could reasonably engender annoyance or skepticism of the pilot's motives on the part of the landowner. It was hoped to demonstrate that UAS operations could help address an ecological issue of local importance without appearing to compromise geographic privacy or creating a nuisance which might generate public opposition to future monitoring efforts using UAS.

The extreme heat and frequent precipitation throughout much of the growing season in southwestern Georgia presented technical challenges for conducting UAS operations. Showers and thunderstorms on and around Lake Seminole are a frequent but unpredictable occurrence, and usually appear with little warning in the early- to mid-afternoon. Even when UAS flights were not prevented by rainfall, this convective weather pattern did at times adversely impact the quality of imagery. Evanescent cloud cover would often cause random and abrupt changes in surface illumination that altered the perceived spectral characteristics of identical features between images in a flight line, and even moderate breezes could create enough surface chop to obscure submerged vegetation. With little shade afforded by the aluminum fishing boat from which operations were conducted and temperatures often in excess of 35°C, there were frequent problems with electronic equipment overheating and malfunctioning or entering failsafe mode. Efforts to shield equipment from direct sun exposure or limit contact with radiative surfaces proved moderately successful; however, even in the shade, high ambient temperatures and humid, stagnant air limited the ability of internal fans and heatsinks to remove waste heat from

sensitive electronics. The UAS itself was not immune to these effects. On multiple occasions, after a few successive flights the UAS would malfunction with an unspecified error message when attempting to transmit the flight plan from the remote control to the UAS. This problem never occurred in cooler weather and would resolve once the aircraft cooled down, which suggested overheating of one or more internal components. The ambient external temperatures during the hottest parts of the day exceeded the 40°C and 35°C maximum operating temperatures of the UAS (DJI 2016), and iPad flight controller (Apple, Inc. 2019), respectively. Survey efficiency therefore benefitted greatly from implementation of a number of heat mitigation strategies. Shading of all electronic equipment was achieved using clamp umbrellas and towels. Direct contact between any batteries, electronic equipment or the UAS with metal surfaces was avoided by interposing white poster board. Only by effectively mitigating direct sun exposure and boosting air flow was it possible to fly the UAS continuously throughout the day in intense summer heat.

Survey Equipment

A DJI Phantom 3 Professional, a lightweight (1.28kg) quadcopter-style UAS, was used for this study, as depicted in Figure 3.3. The standard RGB camera was fitted with a color polarizer lens filter to reduce glare and overexposure from the brightly-illuminated water surface. Modifications were made to the remote control to boost its signal transmission and enable HDMI video output. Live, HD-resolution video could then be viewed through FPV flight goggles at any point in the flight, enhancing situational awareness and the ability to adjust and verify the suitability of camera settings for actual field conditions. While the iPad tablet computer running the flight planning interface did provide a live video feed through the USB to lightning cable, the

playback quality was poor and outdoor lighting conditions created too much glare to visualize the screen clearly. It was also necessary to close the lid of the tablet enclosure for extended periods of time to conserve battery and avoid overheating, which limited its use for flight monitoring purposes. Eight UAS flight batteries, a mobile power source, and a four-bay charging station were sufficient to enable continuous flight throughout the day. Each battery takes approximately one hour to charge at 100 Watts (W). A 400W charger capable of simultaneously charging four batteries was connected by a power inverter to an automotive battery. Using this method, four batteries could be recharged while the other four were used. The maximum number of flights conducted in a single day was 20. Starting with eight charged flight batteries, two automotive batteries provided enough power to charge the additional 12 flight batteries needed. Deep-cycle lead-acid marine batteries were initially used, and while relatively cheap (around \$50USD), they were cumbersome (>28kg each) and their power storage capacity attenuated rapidly before failing altogether at the end of the 2016 survey. They were replaced for the 2017 survey with a lithium ion mobile power supply, which had roughly the same power storage capacity but was smaller, lighter (11.3kg), had an integrated power inverter and sturdy carrying case, but was much more expensive (\$1,000USD). Another viable but costlier solution would have been to purchase a total of 20 flight batteries for a total cost of around \$2,400USD.



Figure 3.3: Photograph of field survey equipment and operating conditions

Survey Design

The survey was designed to maximize daily areal coverage while minimizing conditions that might negatively affect image quality or adherence to the Part 107 operational requirements. All flights were carried out at 120 meters AGL with 100-meter spacing between flight lines. In the 2016 survey, a variety of flight line directions and sensor orientations were evaluated to determine the best combination of parameters. A top priority was to minimize image noise introduced by specular reflectance, the random diffraction of light from the surface of water. Figure 3.4 gives an example of the negative impact that surface reflectivity, sensor angle, and

atmospheric conditions can have on the quality of the resulting orthomosaic imagery. Images taken at nadir were found to have the highest levels of specular reflectance, and greater obliquity resulted in a progressively milder impact, given the same sensor direction and time of day. However, high obliquity imagery is more computationally demanding to process than nadir imagery, and the effective ground-sample distance (GSD) is reduced due to the increased distance between the target and sensor. A 30° oblique angle was determined to provide an optimal reduction in specular reflectance without adversely impacting spatial resolution or processing time.

The UAS model used in this survey did not have the capability to alter sensor direction independently of the aircraft frame and so was fixed with respect to the direction of flight. In order to avoid sun glint, oblique images need to be directed away from the sun, so the flight planner should consider the time of day when choosing flight line orientation. For example, an oblique image facing East would be severely impacted by sun glint in the morning but would not be affected by mid-afternoon. When a mission's flight lines were oriented East to West, the sensor direction had to be manually reoriented to face either East or West depending on the time of day. Such frequent, on-the-fly changes to the flight plans created additional processing difficulties and precluded the development of a standardized, repeatable survey structure. Also, failure of image alignment during photogrammetric reconstruction would frequently occur when oblique images were oriented in opposite directions between adjacent flight lines, particularly if the images contained a substantial number of trees or other vertical elements. It was not deemed efficient in terms of per-flight areal coverage to fly "sideways", orienting the sensor perpendicular to the flight line. Since the UAS video format's field of view is wider side-to-side

(4096 pixels) than top-to-bottom (2160 pixels), the area covered by each flight line is greatly diminished and requires flight lines to be closer together to ensure sufficient side overlap.



Figure 3.4: Striping in an orthomosaic from cloud-induced overexposure

Another component of overall survey efficiency is to minimize the distance between the start and end points of the flight line from the point of takeoff or home point location, therefore utilizing the most battery life for the survey portion of the flight. UAS operations from a boat offered greater flexibility than on land with respect to the location of and transit time between home points. Changing home points every four to six flights was found to be a suitable compromise between the conflicting priorities of maximizing flight battery efficiency and minimizing transit time between home point locations. Figure 3.5 illustrates how the nature of the land cover, and decisions related to flight line and sensor orientation and obliquity are accounted for in flight planning. Figure 3.5(a) is problematic logistically because it is westward facing, which will be compromised by sun glint if flown in the afternoon, transects open water, and is comprised of

multiple short flight lines. Figure 3.5 (b) is optimal because it is north-facing and can be flown any time of day, the lines do not transect a large expanse of open water, and it is comprised of only two lines.

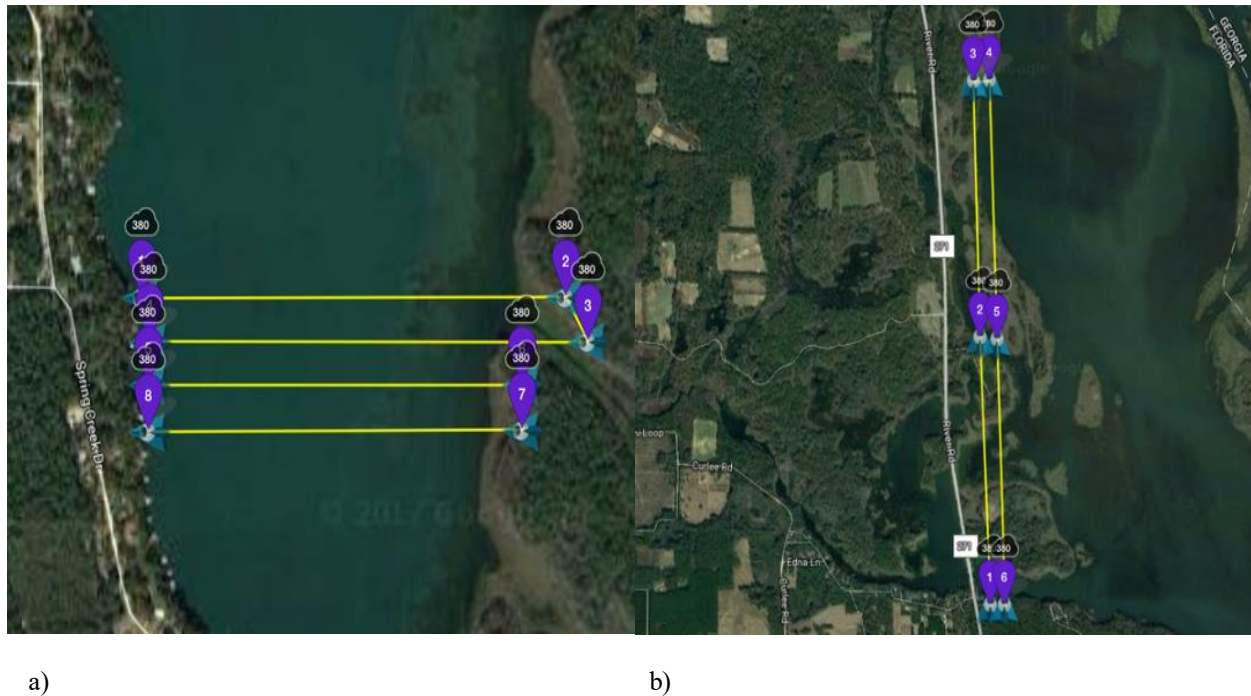


Figure 3.5: Examples of flight line and sensor orientations used: a) a problematic flight design; and b) an optimal flight design

The survey design developed iteratively during the 2016-2017 seasons to address the issues outlined above. The optimal combination of factors determined include: 1) North-South oriented flight lines, 2) northerly sensor direction, and 3) a 30° oblique sensor angle. These were found to offer optimal areal coverage, consistently minimize specular reflectance throughout the day, and the potential for uniform application across the study area. The only exceptions to this pattern were portions of the Flint River arm of the reservoir where a number of factors justified limited deviation in flight line orientation. This arm of the reservoir runs East-West, and vegetated areas along the banks are bifurcated by a large expanse of open water. In some areas, a single East-

West oriented flight on each bank could effectively substitute for several North-South oriented flights, which would mostly cover open water.

Data Acquisition

The UAS sensor used was capable of capturing true-color still images at 12MP (4000x3000 pixels) and video at up to 4K (4096x2160 pixels) resolution, which translates to a GSD of approximately 7 cm when flown at 120 meters above ground level (AGL), near the maximum UAS flying height allowed under Part 107. Still images can be captured at a maximum rate of one of per second, and 4K video at a rate of 24 frames per second (fps). Whereas still images record sensor GPS location in Exchangeable Image File (EXIF) metadata, video frames do not contain any location information. The lack of GPS data and the additional time needed to render still frames are drawbacks to using video, but there are also a number of advantages. While a one-second sampling rate would in general provide enough overlap between successive images to photogrammetrically reconstruct a scene, sometimes a shorter time interval may be required, depending on UAS velocity, flying height, and the nature of the land cover being mapped. For example, images comprised mostly of spectrally-homogenous open water can confound the image matching process unless highly redundant images are available. Unlike still images, video guarantees that the data collected will be sufficient to map a scene under a wide range of operational conditions, eliminating the possible need to re-survey the area, which could be impractical or even impossible.

Although a 4K video frame is lower resolution than a 12MP still image (8.847 million vs. 12 million pixels), this difference is attributable to differing aspect ratios and does not affect the GSD of the resulting image. For this survey, the aspect ratio of 4K video offers a slight

advantage over still images in terms of image width (4096 vs. 4000 pixels), and its reduced height (2160 vs. 3000 pixels) is compensated for by rendering frames with a shorter time interval between images.

A major disadvantage of using video frames is the absence of GPS tags which can be utilized by the photogrammetric software to initialize the coordinate system, scale, and orientation of the model, reduce image alignment time, and simplify the georeferencing process. To address this limitation, a method to extract, format, and append GPS location data to video frames was identified. The UAS flight planning application includes an option within the advanced video settings called “Create Video Caption” which, when enabled, outputs a companion text file in SubRip Subtitle (SRT) file format for each video. During video playback, text from the SRT file, which includes sensor settings (ISO, shutter speed, f-number), time stamp, GPS location, and barometer value (flying height in meters above takeoff elevation) is superimposed on the video and refreshes at one second intervals. The video duration and frame rate from the video metadata are used to pair each extracted video frame with the most-closely corresponding SRT entry. If the frame extraction rate significantly differs from or is offset to the SRT sampling interval, the location of the frame is determined by linear interpolation between the X and Y coordinates of the two closest entries while assuming a constant velocity. The coordinates of each frame are then collated into a table in comma separated values (.csv) format containing four values: file name, longitude, latitude, and flying height. The .csv can then be imported into the photogrammetric software as location metadata. This method presented a number of shortcomings that should be noted. First, locational precision is limited to >10 meters since the coordinate values displayed in the video caption are truncated to 4 decimal places, while EXIF tags from a UAS image are recorded to 12 decimal places. Next, the assumption underlying the

determination of intermediate camera locations based on linear interpolation, namely constant velocity along the flight path, is belied in practice by a feature of the flight planning software used. The software restricts the maximum distance between any two subsequent waypoints in the flight plan to 6,000 feet (1828.8 meters). At each waypoint, the UAS is programmed to decelerate from cruising speed to a stop as it approaches the waypoint before accelerating back to cruising speed. Finally, the SRT to .csv conversion required multiple additional steps and was necessarily more time consuming than automatic EXIF metadata import. A simpler and more user-friendly method to capture location metadata from the UAS flight to aid in georeferencing was determined subsequent to the Lake Seminole surveys. It involves simply taking a few still images at the beginning and end of a survey flight before and after video collection. This takes an insignificant amount of flight time and provides an enormous benefit. Ideally, the still images should be well-distributed throughout the scene to minimize georeferencing error. These few still images, which overlap with the video frames, provide sufficient coordinate system information to georeference the orthomosaic. The referencing results were significantly more accurate, even when the referenced still images were not well-distributed in the scene. Given the comparative ease of this georeferencing method, it is not then necessary to provide location metadata for the video frames through the previously described SRT conversion process.

The process of converting a video to a set of still images is straightforward and may be accomplished using a number of freely-available software programs. Blender Render v.2.69 was used for video frame extraction. A .blend program file template was created to store pre-defined processing and output parameters, and required the user only to select a video file, specify the last frame in the video, and select the folder location and file name prefix for the output still frames. Using a template file for still frame extraction ensured consistency in the parameters

used to process several hundred video files. The frame extraction process can be time-consuming, (60-90 minutes to render frames from a single flight) but is not computationally demanding and can be run on a 32-bit operating system. The processing was distributed across several computers reading and writing from a network attached storage (NAS) device. The frame rendering parameters control image size, anti-aliasing options, color depth, image format, and compression level. No digital filters or alterations to brightness, contrast, or saturation values were made prior to photogrammetric reconstruction. Image size can be the same as the input video resolution (4096x2160p) or downscaled by two to 2048x1080p resolution to minimize processing time. Downscaling images can allow for processing larger image sets on the hardware available with negligible effects on model quality. Frames were rendered at a rate of 1 per second, anti-aliased, and saved as Joint Photographic Experts Group (JPEG) images. The average file size was between 2-3 megabytes (MB). Tagged Image File Format (TIFF), Portable Network Graphics (PNG), and Bitmap (BMP) image file formats were all evaluated in terms of their relative size and image quality. There was little apparent difference in image quality between a 2MB JPEG and a 32MB BMP rendering of the same frame, so it was decided to use smaller JPEGs. Since random-access memory (RAM) usage during photogrammetric reconstruction is a limiting factor and proportional to aggregate image file size, smaller individual files enable larger and higher quality models to be generated with the available amount of RAM. The SRT captions were then converted into a .csv which used the same naming convention and sampling rate as the video frames, so that they can automatically be assigned to the correct image in the photogrammetric processing program.

Photogrammetric Processing

Structure from Motion (SfM) photogrammetry was then performed using Agisoft Metashape Professional software (formerly known as Agisoft Photoscan). While photogrammetry has been used for over a century to map terrain and elevations (Frank and Manten 1969), SfM is a recent development resulting from application of machine-learning and computer vision algorithms to traditional photogrammetry. SfM is a much more powerful and applicable than traditional photogrammetry because it enables the computer to solve the camera location for each image, whereas in traditional photogrammetry the sensor location and orientation had to be known a priori, and the calculations required to reconstruct images other than nadir aerial images were prohibitively difficult. The SfM process produces a fully reconstructed three-dimensional (3D) scene from a series of overlapping 2D images. The process uses machine-learning algorithms and iterative bundle-block adjustment procedures to identify corresponding features in overlapping images and solve for the camera locations and assign all matched points a coordinate in 3D space and RGB color. Using this initial alignment, an exhaustive set of point matches is computed, resulting in a dense point cloud. A triangulated mesh model is then generated from the dense point cloud. The mesh faces are assigned an RGB color based on the average of the vertex colors from the dense point cloud. An image texture can also be generated by projecting the source images onto the mesh model. SfM can yield incredibly detailed and photorealistic models (Wang et al. 2019), and can be used to map and represent a range of objects from the microscopic (Plisson and Zotkina 2015) to the landscape scale (Smith, Carrivick, and Quincey 2016).

The workflow to perform SfM may vary depending on the limitations of computer hardware, desired model quality, and size of the project. A general workflow used in this study is depicted

in Figure 3.6. The hardware specifications of the workstation(s) to be used in photogrammetric processing, including central processing unit (CPU) core count and base frequency, graphics processing unit (GPU) core count, and available random-access memory (RAM) all play a role in determining the maximum achievable model size and reconstruction quality. Reconstruction was attempted initially using a single workstation equipped with 16 GB of RAM and a quad-core CPU with an integrated graphics card. This system was only able to process image sets, referred to as chunks, of 100-200 images within a reasonable time frame (subjectively, less than 24 hours). Frequently, protracted photogrammetric reconstruction on a very large dataset would result in program or computer crashes, necessitating repetition of the entire process. This is both frustrating and inadvisable from an efficiency standpoint. Computer calculations for the bundle block adjustment and dense point cloud generation can be greatly accelerated by the addition of even a single dedicated GPU. Photogrammetric processing using only CPU or an integrated GPU is not recommended. The computer hardware limitations described led the initial survey dataset to be processed in several hundred chunks of 100-200 images each. Images were output during video extraction with a file nomenclature and folder structure organized by flight ID and flight line sequence number. Prior to executing the reconstruction process, overlapping images were loaded manually to chunks by referencing the flight plans. Image thumbnails were visually scanned, and images containing mostly open water that would have insufficient tie points to align properly were disabled so that they would not be used in the alignment process. Where intervening open water bifurcated a flight line into two or more spatially discontinuous segments, the chunk would be duplicated and processed separately. The chunk nomenclature would be amended to reflect a sub-flight division (i.e., 2016_Flight37_Line1_Segment1). This was

necessary to keep track of the myriad chunks to ensure that they would align with the appropriate adjacent chunks in subsequent steps.

Processing very large scenes in many small increments is not recommended. Alignment and union of adjacent chunks based on dense cloud comparison caused distortions or failed altogether and the many chunks became progressively more tortuous to keep track of. However, given initial hardware limitations, this was the only option available, and orthomosaics of up to 2,000 images were ultimately produced using this method, so it might be sufficient for smaller study areas.

In order to efficiently process the very large image sets (over 115,000 images total) this survey produced, more numerous and powerful computational resources were required. Using Agisoft Metashape, each processing step can be distributed amongst a number of computers in a local network which is much faster and more efficient than with a single computer. A multi-workstation and NAS setup was assembled specifically for the purpose of processing this survey imagery. Four workstations with high available RAM (32-64GB), CPUs with high base frequency (>3.0 GHz) and core-count (>10), and multiple graphics cards were networked to process the surveys. The workstations were custom-built for photogrammetric processing. The marginal impact of adding graphics cards on overall processing time diminishes with each additional card, so with four workstations and eight available graphics cards, the optimal configuration is for each to contain two GPUs. With this hardware setup, no maximum imagery quantity threshold was identified for the number of images that could be processed in a single chunk for the image alignment step. The largest chunk contained over 21,000 images and aligned in under four hours. Now, instead of having to divide flights into multiple chunks due to computational limitations, twenty or more flights could be processed in a single chunk. The

image alignment step for an entire annual survey dataset can be accomplished in a single day in three to four chunks, which can be duplicated and sub-aligned where spatial discontinuities exist. In cases where large numbers of images failed to align due to predominance of open water, the chunk can be duplicated, the aligned images removed, and the previously unmatched images aligned. This was faster and lessened the opportunities for human error in chunk compilation and processing. Following the alignment step, the sparse point cloud was manually evaluated and modified. Generally speaking, the initial alignment on large projects does not match all of the photos, and sometimes spurious image alignments miscalculate the camera position, which cascades into subsequent calculations, warping what should be a planar surface into an involuting nautilus shell-like formation. The frequency of this behavior is less frequent (but not absent) when image GPS tags are applied and is greater with low tie point land cover types, such as open water. When images do not initially align correctly or at all, they may be selectively aligned or refined using the ‘Align Selected Cameras’ command. If there is a spurious alignment, alignment for certain or even all cameras can be reset and realigned in a stepwise fashion. Starting by aligning a small subset of images covering an area high in textural variety and verticality seemed to more reliably form a planar initial alignment. Conversely, starting alignment with poorly focused images, large amounts of open water, and homogenous land cover types tended to enhance undesirable curvilinearity in the model.

For each chunk, the user should also verify the Reconstruction Region, the bounding box delimiting the area to be reconstructed, is positioned appropriately. The Reconstruction Region is initialized during the image alignment step and does not change with subsequent manual image alignment. The ‘Reset Region’ function may cut off the edges of long or narrow point clouds. The reconstruction region must be resized manually in these cases.

Once all cameras are satisfactorily aligned, the ‘Optimize Cameras’ tool is used to correct for the effects of lens distortion on the point cloud using Brown’s distortion model. The UAS camera lens distortion coefficients for Brown’s distortion model were calculated by collecting numerous images of a computer monitor displaying a black and white checkerboard pattern from multiple angles, adding these images to a chunk, and applying the ‘Lens Calibration’ tool. The coefficients to Brown’s distortion model are calculated and then applied to the survey images, and the ‘Optimize Cameras’ tool is run. Following initial optimization, the point clouds were then filtered and thinned according to statistical measures of each point’s accuracy using the ‘Gradual Selection’ tool in Metashape. The goal of tie point filtering is to increase the accuracy of the tie points used to reconstruct the dense cloud, eliminating noise and roughness in the reconstructed surface and resulting in a better model. Metashape analyzes tie points, common features automatically identified on multiple images, and scores each point according to its reconstruction uncertainty, projection accuracy, and reprojection error. Points with high reconstruction uncertainty were eliminated first, then cameras were optimized. Then, error values for the remaining points are then automatically recalculated. The same steps are applied to the projection accuracy and reprojection error. Points with a value higher than a specified target level are selected and removed. The target levels for each parameter are empirically derived (Gatewing 2017). It is preferable to remove tie points in multiple iterations rather than a single step (Mayer, Pereira and Kersten 2018). In this situation, too many tie points may be removed, leading to partial or null results in the dense cloud step. This effect was pronounced in areas mixed with deeply submerged vegetation and open water. It is better to include some inaccurate points than remove points beyond a critical threshold (Röder, Hill, and Latifi 2017). When to terminate iterative point removal should be assessed on a case-by-case basis and the point cloud

should be inspected prior to reconstructing the dense cloud to verify that sufficient tie points remain.

When optimization yields a satisfactory alignment, a dense point cloud is reconstructed. The tie points are used as a basis for the reconstruction and all possible matching points are calculated, yielding the dense point cloud. Medium or low quality settings are recommended for chunks with more than 5,000 images, and very low quality for those with greater than 5,000 images.

If scene topography is uniform or the structure of vertical elements are irrelevant to the task, it is possible to skip dense cloud generation altogether and create a mesh directly from the sparse cloud. This model will have a much lower polygon count than if a dense cloud were used, but it may be beneficial to produce a rapid initial result to check alignment and texture quality prior to processing at a higher quality level.

Elevation data, including DEM and bare-earth digital terrain models (DTMs) can be generated in Metashape following dense cloud generation. DEMs are used in subsequent steps to identify and mask out areas of the orthomosaic that are irrelevant to the analysis, such as the trees and riparian vegetation on islands and along the shore. A DTM can save processing time during mesh generation by excluding above ground elements from reconstruction. The following steps are used to exploit the DTM. The ‘Classify Ground Points’ tool assigns points to the ground class if the point lies below a threshold angle from the lowest points within a specified region of the model. The default values for the Classify Ground Points tool provided satisfactory results for this step. Since the reservoir’s surface is virtually flat, above water points are easily classified. Once the dense cloud is classified, a mesh can be generated using ground points only. The ‘Build DEM’ tool is then run using the ground-points-only mesh, which yields a DTM. Topographic contours are then generated from the DEM. The contour best representing the reservoir’s surface

is selected both visually and numerically. The vertical coordinate system defaults to meters AGL, with zero being the UAS starting elevation. Since the UAS takeoff elevation is just above the water, the shoreline boundary contour was assumed to be somewhere close to zero. Multiple contours for a narrow range (-1 to 1 meters) were generated and overlaid on the orthomosaic in Metashape to visually identify the contour that best fit the shoreline, which was then exported as a polygon shape file to mask land area in the orthomosaic prior to image segmentation and classification.

Once the 3D model and DEM have been generated, the final step in the photogrammetric reconstruction process is to build an orthomosaic and export it to a GIS software for further image analysis. When building the orthomosaic, it is recommended to use a mesh generated with the highest quality setting possible for a given model size. For very large datasets (>5,000 images), Metashape is prone to freeze or crash when the quality level is set above medium (high or ultra-high quality settings). Metashape creates orthomosaics by projecting the texture of the 3D model onto a plane lying orthogonal to the top-down view. The orientation of the projection plane is calculated automatically for every model using the georeferencing data. In the event the mesh lacks or has incomplete georeferencing data, the projection plane does not always correspond well to the model, which can yield a warped orthomosaic. When the model lacks image metadata, the 'Reset Region' and 'Rotate Object' tools can be used to correctly orient the model with respect to the view angle. When image metadata is present and this issue occurs, the tools to rotate or transform the 3D model are disabled. This situation must then be resolved by rotating the model in the viewer window to the desired top-down view and specifying 'Current View' instead of the default 'Top-Down' option in the Build Orthomosaic dialog box. This issue was infrequent when the model contained image location metadata, but did still occur in some

cases. For these cases, it was hypothesized that the misalignment arose from the program assuming in the absence of sensor orientation data that the images were taken at nadir, when they were in fact at an oblique angle. Importing sensor orientation values and re-processing the dataset could potentially resolve the issue for affected models. Once the orthomosaic is generated and inspected in Metashape, it is exported for further analysis in ArcMap GIS software. The orthomosaics were exported in GeoTiff format, since it is a lossless format and stores georeferencing data in the same file as the image. The orthomosaic's reference data were transformed from a geographic coordinate system (WGS 1984) to a projected coordinate system (WGS 1984 UTM Zone 16N) prior to export. Products of this photogrammetric reconstruction workflow were a dense point cloud, 3D model, georeferenced orthomosaic image, DEM, DTM, and topographic contours. This process could produce additional data products which could be used for visualization and analysis purposes, which will be addressed in Chapter 5.

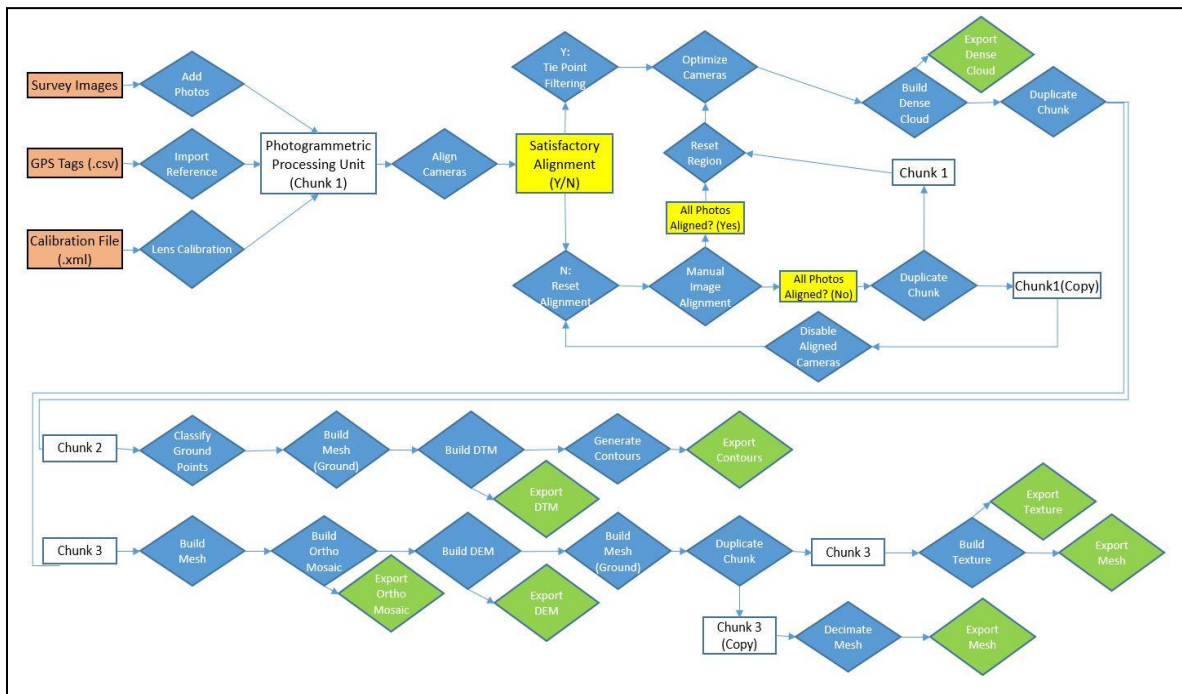


Figure 3.6: Diagram of the photogrammetric reconstruction workflow used

Geographic Object-Based Image Analysis (GEOBIA)

A geographic object-based image analysis (GEOBIA) process was then performed on the photogrammetrically-generated orthomosaics. The GEOBIA process consisted of three stages: image segmentation, training area selection, and image classification. Image segmentation involves partitioning a raster into groups of pixels with similar characteristics, known as segments, that represent discrete image objects. Raster segments are generated based on evaluation of statistical measures of each pixel's spatial relationship and spectral similarity. Segment size, the minimum number of pixels needed to constitute a discrete segment, varies according to the relative importance of spectral detail, spatial detail, and minimum segment size. The segment size parameter was determined to be the most important factor in achieving an appropriate segmentation scale, echoing the findings of Kim et al. (2014). When the segmentation scale parameter is set to one, processing time is increased, a larger set of training samples is required by large amounts of within-class spectral variability, since even the smallest individual object is composed of numerous segments. At the opposite extreme, a large minimum segment size in the thousands risks obscuring smaller, more dispersed objects, such as floating leaf vegetation which are often not spatially contiguous. This also confuses the training selection because the merged segment color will potentially include pixels from a number of different classes. Large minimum segment sizes were found to poorly differentiate between open water and deeply submerged macrophytes, leading to poor classification accuracy. A minimum segment size of 16 was determined iteratively to be the most appropriate scale for identifying floating leaf vegetation and limiting the overestimation of open water area. Figure 3.7 illustrates the impact of the minimum segment size parameter on segmentation results by showing an area

of mixed macrophyte and floating leaf vegetation at progressively greater minimum segment sizes.

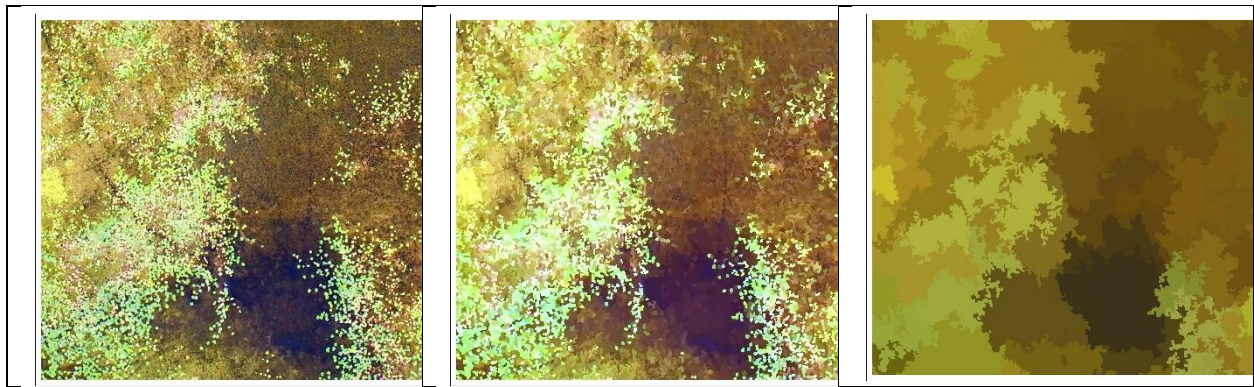


Figure 3.7: The impact of minimum segment size on segmentation results, showing minimum segment sizes, from left to right, of: 1, 16, and 1,600

Once a segmented raster is generated, a training sample file is created manually through image interpretation. Training areas are a subset of segments selected to best represent a given vegetation or land cover type, and are used as the basis for classifying the rest of the segmented image. Classification accuracy is highly dependent on the quality of the training area selected. The training segments should be comprehensive and exhaustive, such that every object in the image is represented by a class in the training sample, and each spectral variant of an object is represented by its own class. This may necessitate that a single vegetation class be initially comprised of multiple classes which are merged following image classification into a single class. The training set should contain at least twenty discrete segments for each class (Green 2017), but in practice it was found to require a much higher number of segments, to avoid a software-generated warning message about low sample size, and potentially poor classification. A sample size of around 150 segments was used for the classification presented herein. It is important to keep in mind the desired or attainable level of detail of the classification scheme when selecting training areas. For example, broadly inclusive training segments would

be appropriate if the end goal were to simply determine presence/absence of vegetation. A progressively more discriminating selection is required to distinguish between vegetation types (such as SAV vs. floating leaf), individual species, or phenologic stage of an individual species. Training areas must also account for within-class spectral variation caused by differences in illumination, such as shadows or sun-glint. These areas should be classified separately and merged with the appropriate vegetation class following image classification.

Image classification is accomplished by applying the training results to an algorithm which then determines the spatial and spectral attributes of each class and categorizes the entirety of the segmented image accordingly. The algorithms used were Maximum Likelihood Classifier, ISO Cluster Classifier, Random Forest (also referred to as Random Trees in ArcGIS software), and Support Vector Machine (SVM).

The data produced by Metashape were imported into ArcMap 10.5 for the GEOBIA analysis. The images were clipped to exclude land and riparian species from the classification, greatly simplifying analysis and reducing processing time, as land classes exhibited greater within-class spectral variability and were not relevant to the research objective. The segmentation and classification steps were then applied in a batch process to each orthomosaic using the ModelBuilder function. Processing time varied according to the size of the input raster, specified minimum segment size, as well as the number of input bands, and ancillary raster inputs included. Following segmentation, training sample files were manually produced for each raster. Differences in scene illumination, phenological stage and relative abundance and assemblage of classes prevented the uniform application of a single training area file to multiple orthomosaics. While in some areas, individual species and phenological stage were readily identifiable from the imagery, spectral similarities between certain species, in particular submerged non-hydrilla

macrophytes, resulted in unreliable classification results at the species level. Therefore, although the training samples were selected at a fine level of detail, including species and phenology, it was decided for the final classification map to reclassify and merge classes to a broader classification hierarchy. This improved classification accuracy and provided a consistent classification scheme with previous in-situ and remote sensing-based vegetation surveys in the study area. Therefore, with the exception of hydrilla, the classification scheme used in the final classification map corresponded to the Plant Community column of the classification scheme presented in Table 3 below. Although the classification was generalized, the results were more detailed in terms of spatial coverage than previous surveys.

Land Cover	Presence/ Absence	Plant Community	Species	Zonal (Depth)	Phenology
Terrestrial					
Aquatic	Open Water			Shallow Deep	
	Vegetation	Macrophyte	Hydrilla Pondweed Milfoil	Emergent Submergent	Healthy Senescent Bloom
		Floating Leaf	Water hyacinth Waterlily American lotus	Emergent	Healthy Senescent Bloom
		Algae	Lyngbya Chara	Emergent Submergent	

Table 3: Vegetation Classification Scheme

Once the training samples were created, they were input along with the segmented raster to train multiple pixel- and object-based classifiers, including the Maximum Likelihood Classifier, Random Trees Classifier and Support Vector Machine Classifier. In addition, an unsupervised pixel-based ISO cluster classification was performed on the unsegmented raster. Following classification, classes were merged using the 'Reclassify' tool from the ArcMap 3D Analyst Extension according to the above-mentioned classification hierarchy. Five classes were ultimately created in the final classified maps: floating leaf vegetation, hydrilla, mixed macrophyte, lyngbya, and open water. Due to between-class confusion, it was decided to merge mixed macrophyte and lyngbya classes, yielding four classes. Following reclassification, accuracy assessment for each of the classified maps was conducted. 200 randomly-generated accuracy assessment points (50 for each class) were placed within the boundaries of the segmented raster using an equalized stratified random sampling scheme. The map classification values for each point were compared to a ground truth classification value, which was determined by manual interpretation of the unsegmented raster. From these data, confusion matrices were generated using the 'Compute Confusion Matrix' tool, which reported user's accuracy and producer's accuracy for each class, overall model accuracy, and Kappa coefficient for each classifier.

Chapter 4

Results

This study sought to 1) use a consumer-grade UAS to collect remote sensing data of aquatic vegetation in Lake Seminole, Georgia at multiple time periods and under varied phenological and atmospheric conditions; and 2) use these data to classify and map emergent, submerged, and free-floating vegetation. Geographic object-based image analysis was used to delineate and classify aquatic vegetation at the plant community level. It was intended to assess whether this method would constitute an improvement over alternative survey methodologies in detecting inter- and intra-annual changes in vegetation coverage for ecological monitoring and reservoir management.

The orthomosaic imagery (~7cm spatial resolution) generated from the 2016 survey is presented in Figure 4.1. An unsupervised pixel-based ISO cluster classification was performed for each orthomosaic and amalgamated into one classified map of vegetation over a 38 km² area of Lake Seminole (Figure 4.2). Due to the fact that a different training set would need to be applied to each orthomosaic for a supervised image classification, a reservoir-scale map of vegetation using supervised classification was not completed. This will be addressed further in Chapter 5. Figure 4.3 depicts supervised classification results for a subset of the reservoir. This 507-hectare site, known locally as Sealy's Point, was selected due to its central location in the reservoir between the Spring Creek and Flint River arms and its high diversity of vegetation assemblages, including hydrilla dominant, floating leaf dominant, and heterogenous areas, as well as open water of different hues. Essentially all of the vegetation classes present in the reservoir are depicted in this

single orthomosaic, minimizing spectral variation due to atmospheric conditions on multiple flight days. The results of a previous in-situ vegetation classification survey (Shivers et al. 2018b) are shown in Figure 4.4 to provide a comparison between the results of this survey and previous survey methods. Figure 4.5 shows the UAS orthomosaic (a) and unclassified segmented raster (b) of Sealy's Point. The supervised and unsupervised vegetation classification results for a portion of the study area are presented in Figure 4.6 (a-d). In general, *lyngbya* was not reliably differentiated in the ISO cluster classification, and so this class was merged with mixed macrophyte in Figure 4.6 (b). The results of the accuracy assessment are presented in Table 4. Overall, Random Forest was found to provide the best classification accuracy (78.5%). The classification accuracy for the highest-performing model was slightly lower but in the same range as Husson et al. (80.4%), Tung-Ching and Chou (90%), and Kim et al. (91%).

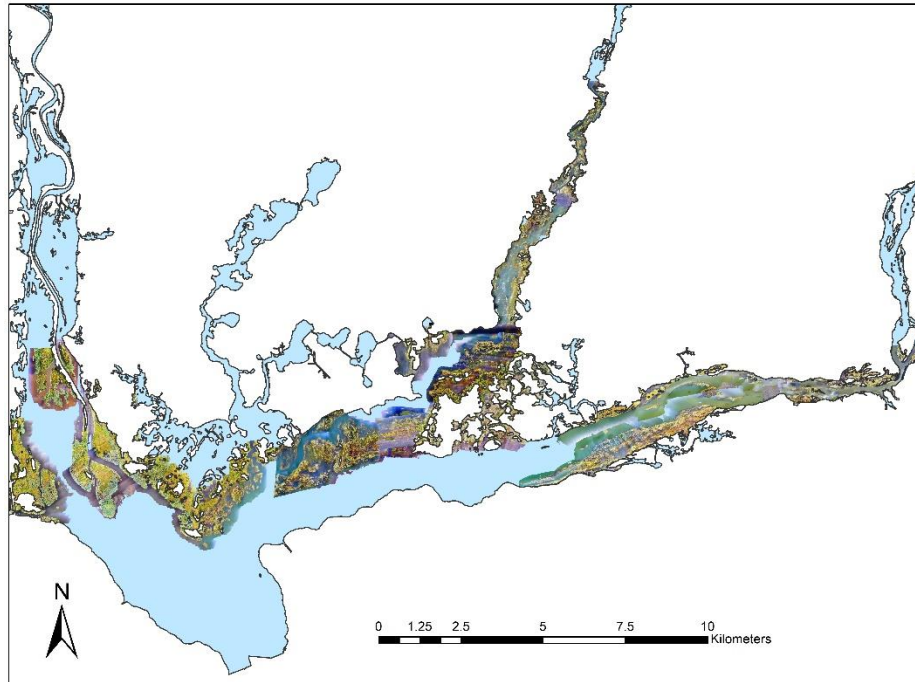


Figure 4.1: UAS orthomosaic coverage of Lake Seminole in 2016

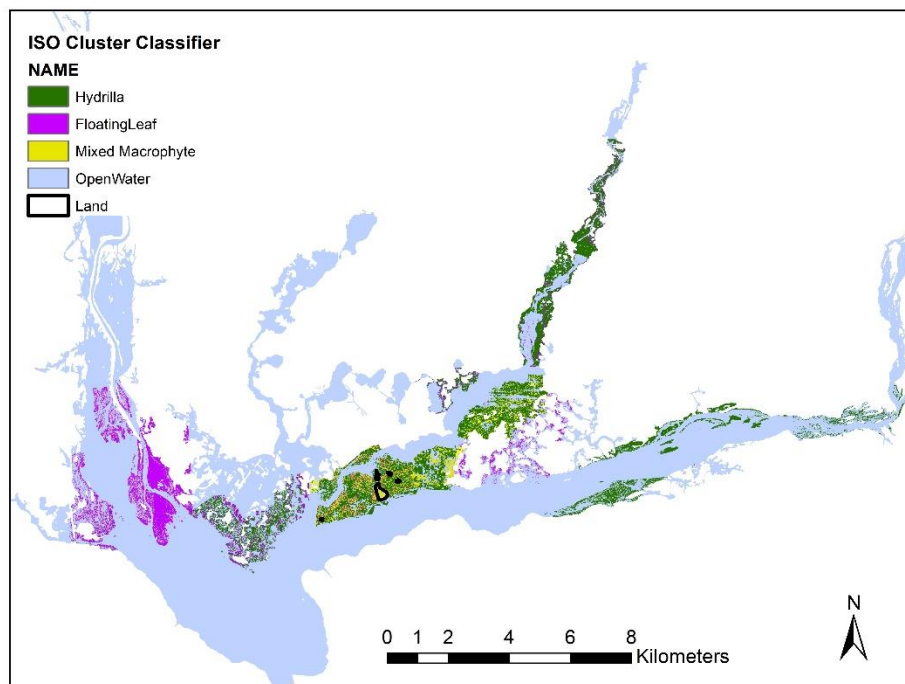


Figure 4.2: Unsupervised ISO classification of vegetation in Lake Seminole

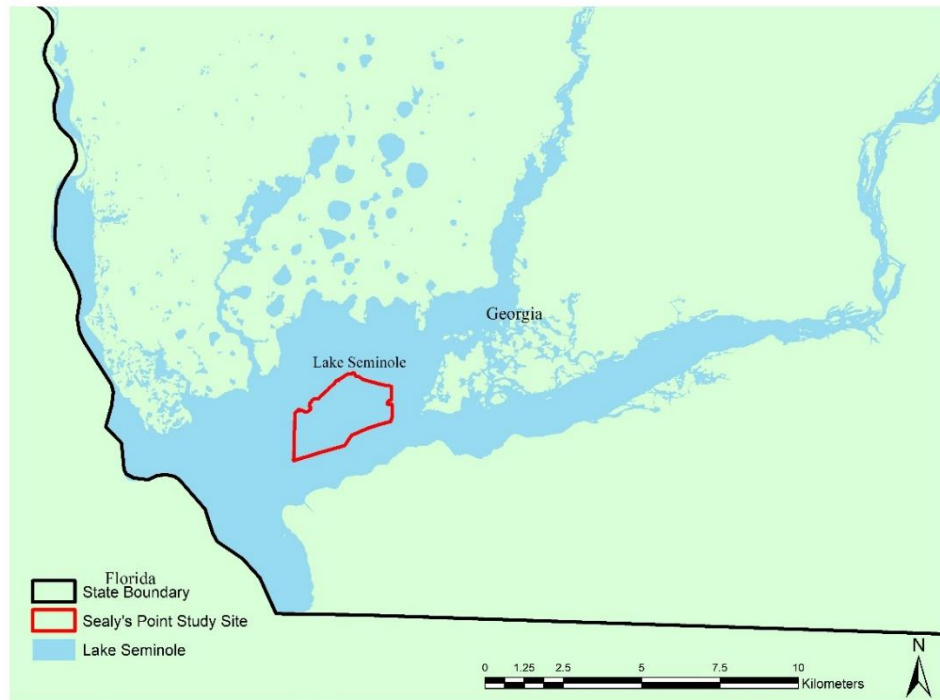


Figure 4.3: Map of Sealy's Point vegetation classification test area

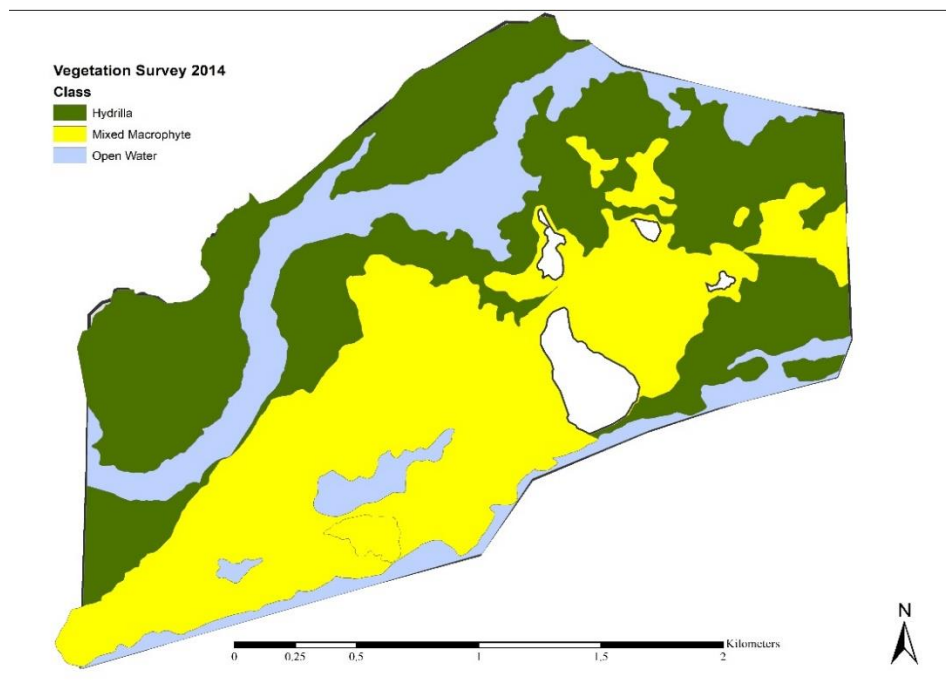


Figure 4.4: Map displaying the results of Shivers' 2014 vegetation survey of Sealy's Point

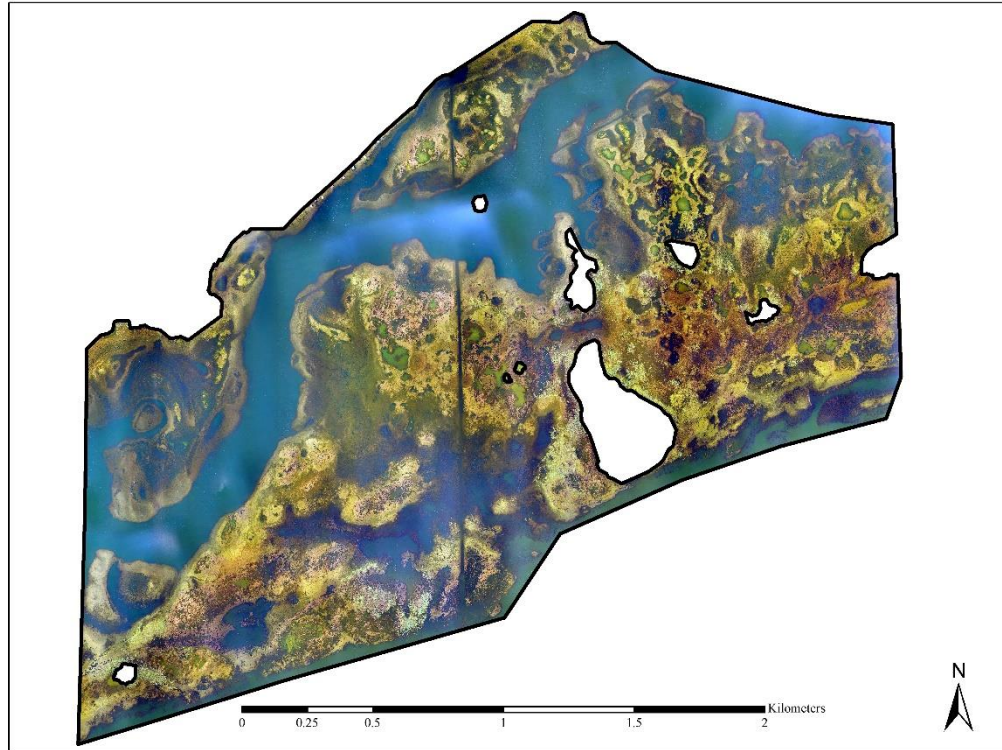


Figure 4.5 (a): 2016 Unclassified segmented orthomosaic image of Sealy's Point

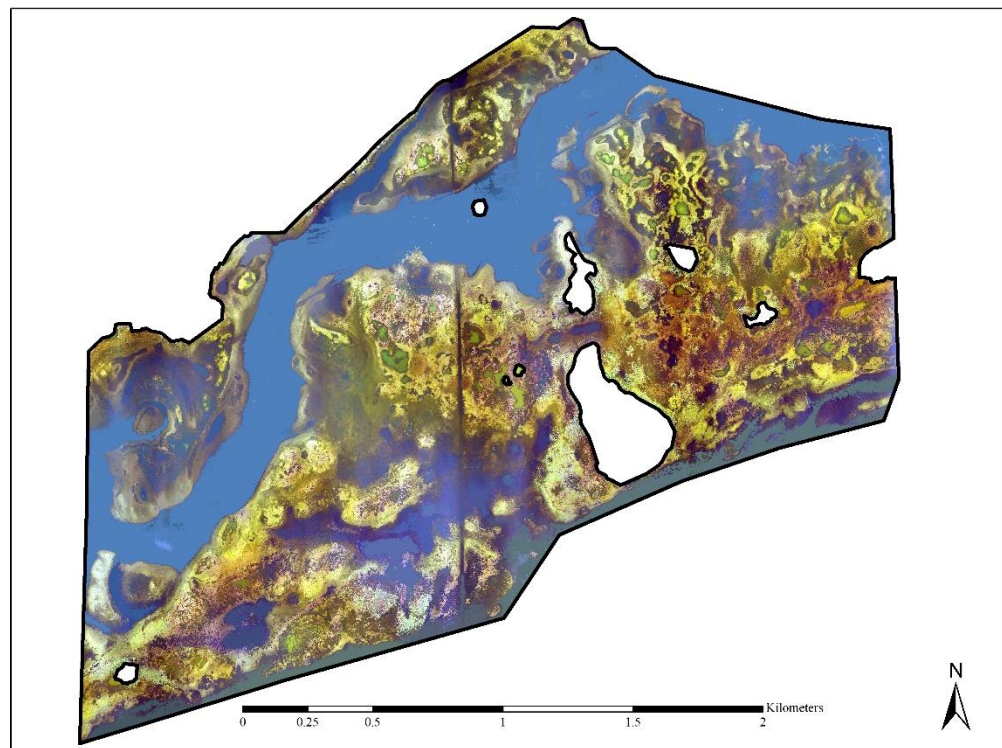


Figure 4.5 (b): Unclassified segmented raster of Sealy's Point

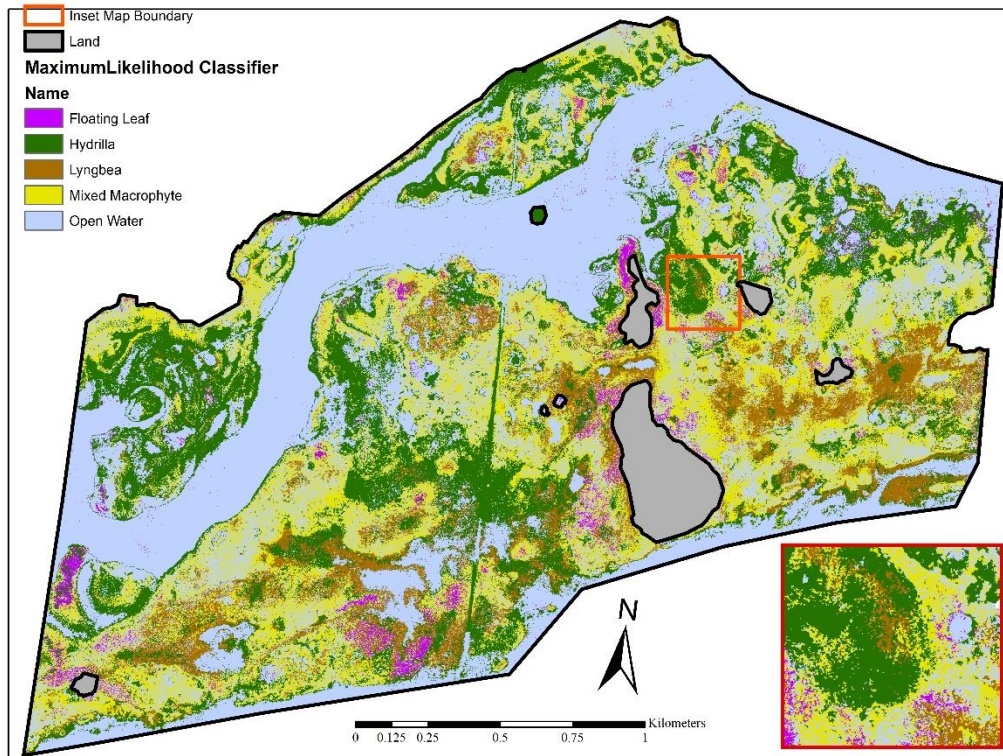


Figure 4.6 (a): Supervised Maximum Likelihood Classifier of Sealy's Point

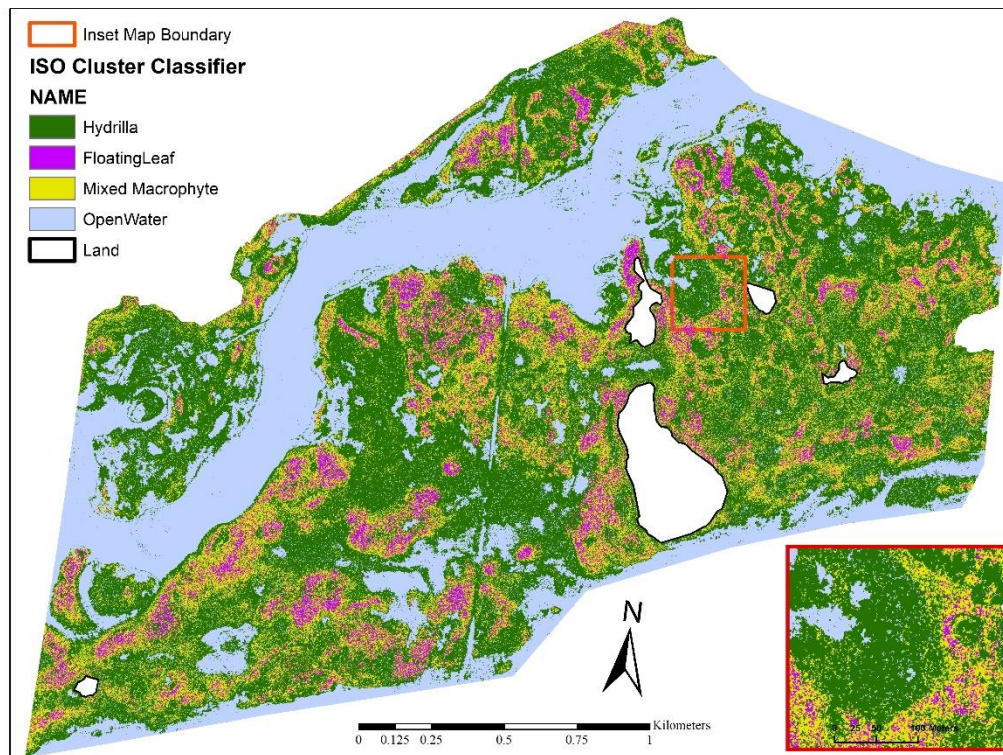


Figure 4.6 (b): Unsupervised ISO Cluster Classifier of Sealy's Point

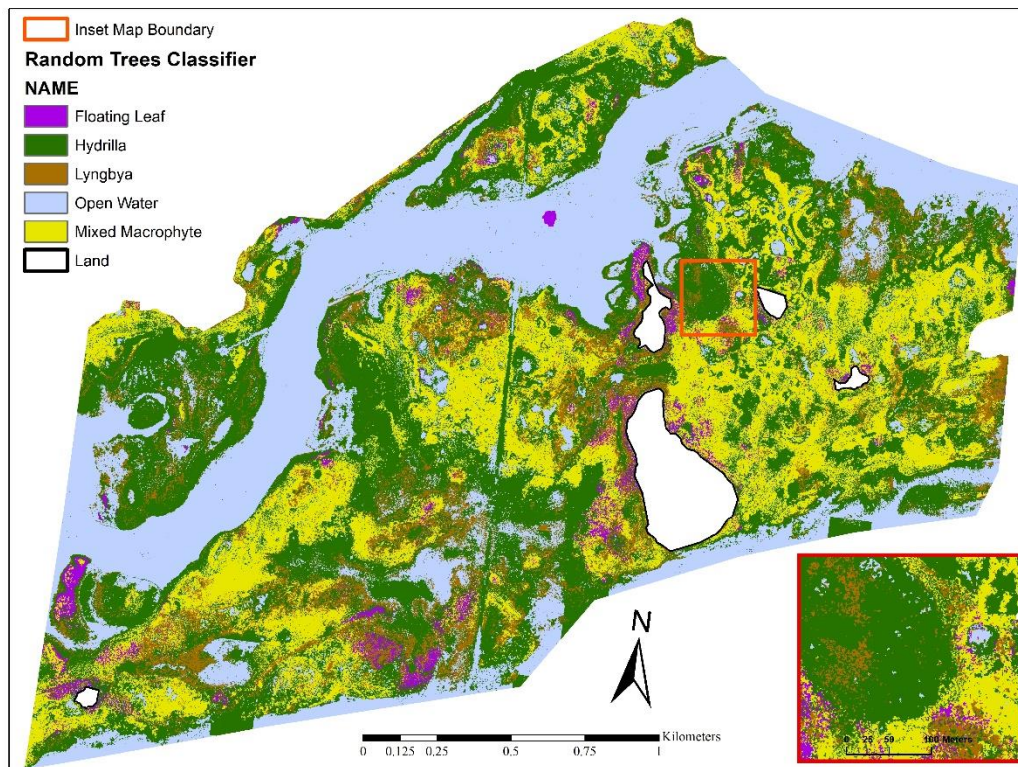


Figure 4.6 (c): Supervised Random Forest Classifier of Sealy's Point

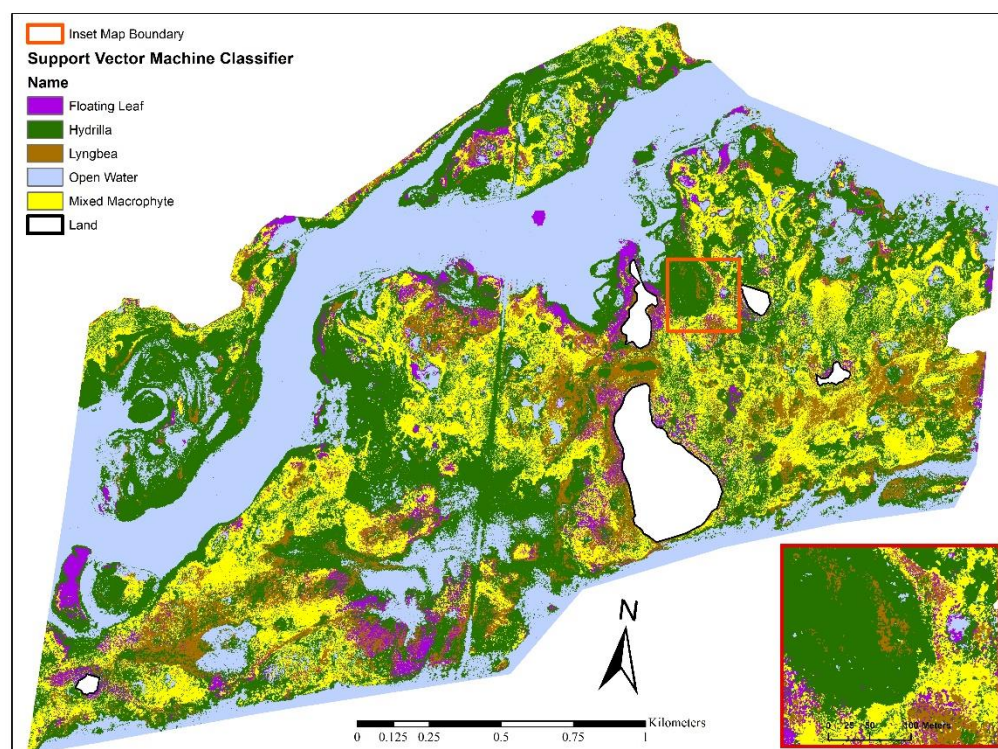


Figure 4.6 (d): Supervised Support Vector Machine Classifier of Sealy's Point

a) Confusion Matrix for Maximum Likelihood Classifier

Class Value	Floating Leaf	Hydrilla	Mixed Macrophyte	Open Water	Total	User's Accuracy
Floating Leaf	3	0	3	0	6	0.5
Hydrilla	0	17	0	0	17	1.00
Mixed Macrophyte	6	30	54	1	91	0.593
Open Water	1	23	24	38	86	0.442
Total	10	70	81	39	200	
Producer's Accuracy	0.300	0.243	0.667	0.974		0.560
Kappa						0.372

b) Confusion Matrix for ISO Cluster Classifier

Class Value	Floating Leaf	Hydrilla	Mixed Macrophyte	Open Water	Total	User's Accuracy
Floating Leaf	8	4	11	0	23	0.348
Hydrilla	2	39	32	3	76	0.513
Mixed Macrophyte	8	17	24	1	50	0.480
Open Water	0	14	2	35	51	0.686
Total	18	74	69	39	200	
Producer's Accuracy	0.444	0.527	0.348	0.897		0.530
Kappa						0.341

c) Confusion Matrix for Random Forest Classifier

Class Value	Floating Leaf	Hydrilla	Mixed Macrophyte	Open Water	Total	User's Accuracy
Floating Leaf	7	0	2	0	9	0.778
Hydrilla	0	41	5	3	49	0.837
Mixed Macrophyte	3	20	74	1	98	0.755
Open Water	0	9	0	35	44	0.795
Total	10	70	81	39	200	
Producer's Accuracy	0.700	0.586	0.913	0.897		0.785
Kappa						0.679

d) Confusion Matrix for Support Vector Machine Classifier

Class Value	Floating Leaf	Hydrilla	Mixed Macrophyte	Open Water	Total	User's Accuracy
Floating Leaf	6	3	5	0	14	0.429
Hydrilla	0	31	12	1	44	0.705
Mixed Macrophyte	4	25	63	1	93	0.677
Open Water	0	11	1	37	49	0.755
Total	10	70	81	39	200	
Producer's Accuracy	0.600	0.443	0.778	0.949		0.685
Kappa						0.539

Table 4: Confusion Matrices for a) Maximum Likelihood Classifier b) ISO Cluster Classifier c) Random Forest Classifier and d) Support Vector Machine Classifier

The results indicate that with the UAS image data of Lake Seminole, machine learning classifiers outperformed pixel-based classifiers, (53% and 56% overall accuracy for pixel-based classifiers vs. 78.5% and 68.5% for machine learning classifiers). The range of Kappa values ranged from 0.372 for ISO Cluster which was the lowest, to Random Forest which had the highest Kappa value (0.679). The ISO cluster classifier greatly overestimated the abundance of floating leaf compared to all the other classifiers. Random Forest had the highest overall accuracy (78.5%), while the ISO classifier had the lowest (53.0%). The Maximum Likelihood classifier greatly under-represented hydrilla, so although it had a 100% producer's accuracy for hydrilla, user's accuracy was 24.3%. Overall, Random Forest performed the best with identifying hydrilla (58.6% user's and 83.7% producer's accuracy).

Given the very high resolution of the imagery and the ability to distinguish individual species visually, the overall accuracy of the classified maps is lower than anticipated. There are a number of factors that are believed to impact classification accuracy. This survey was limited by

the available sensor to RGB spectral bands, unlike other studies where an NIR band was included. The inclusion of NIR would be expected to substantially improve accuracies, perhaps even comparable to accuracies of 90% and above, as reported by Tung-Ching and Chou (2014). Other relevant factors include overexposure of senescent plant material, the proliferation of *lyngbya*, spectral variation (real and atmospherically-induced), phenological differences, and similar spectral signatures and growth form between macrophytes. The relative impact of these factors on the accuracy of the classified map are scale-dependent; that is, the larger the geographic area mapped, the greater the spectral variability that is introduced in the data collection process. However, the vegetation extent identified in this study correspond well to the 2014 vegetation map of Sealy's Point produced by Shivers (Figure 4.4), and provide a considerably higher level of detail.

The results of this study support the assertion by Husson et al. (2014) that UAS-based remote sensing presents “*great potential for lake and river vegetation identification and mapping at the species level, as well as for abundance estimates*”; however, the moderate classification accuracy achieved in this study suggests that more work still needs to be done to establish best practices in data acquisition and processing to minimize the sources of classification error that were identified.

Chapter 5

Discussion and Conclusion

This study demonstrated the ability to utilize a small, quadcopter-style UAS to conduct ecological monitoring of an extensive geographic area in subtropical climate conditions. Chapters 1 and 2 provided context and a rationale for the relevance and suitability of the proposed study, a review of relevant literature, and research objectives. Chapter 3 outlined a workflow for collecting and processing UAS video to create orthomosaic imagery of a reservoir in southwestern Georgia, and use this imagery to map aquatic vegetation at the plant community level. It also discussed complications which arose and proposed methods to address those complications. Chapter 4 presented the results of these efforts in the form of classified vegetation maps and associated confusion matrices, and provided a comparison with an in-situ survey of the same area. This chapter will relate the results of this study to the literature, assess the limitations of the study and propose improvements to future studies.

Limitations

A number of shortcomings in the survey design and implementation limited the ability of this study to address intra- and inter-annual changes in aquatic vegetation coverage. The extent of the study area was ambitiously large and tested the operational limits of the equipment as well as the remote pilot. Over the course of many days of transporting heavy equipment to remote locations and operating in extremely hot and unpredictable weather, there were gaps in data acquisition attributable to human error and equipment failure.

A noteworthy difference between this study and previous aquatic vegetation surveys using UAS-based remote sensing data is the data volume, and the methods to solve operational, organizational, and computational challenges inherent in working with Big Data. Over 115,000 images were processed in this study, some in chunks of over 20,000 images, much larger than the mosaics of 200-300 images created by Husson et al. (2014) and 100-250 images by Flynn and Chapra (2014). This study demonstrates the feasibility of processing much larger image sets, and therefore larger geographical areas, than previous studies. The surveys generated almost one terabyte (TB) of video files, all of which had to be transferred, renamed, and rendered into still images, and at each stage the integrity of the data is vulnerable to small mistakes. For example, an incorrectly entered flight name when rendering still frames could overwrite data from another flight, and the mistake might not be caught until the image matching failed during photogrammetric reconstruction. Correcting mistakes like this were time-consuming and difficult, even when the same person flew the imagery and processed the data; it could be much harder to identify and fix such errors in an organizational setting where multiple people are working on different stages of the process at different times.

Discontinuities and gaps in the data were also caused in a number of areas where the photogrammetric process failed to align the images correctly, particularly in predominantly open water areas. Additionally, there was insufficient understanding of how variations in phenologic and atmospheric conditions would affect the ability to consistently segment and classify the imagery in order to make meaningful comparisons between years. Where overlapping coverage between subsequent years did exist, imprecise georeferencing (positional errors generally ranged from 10 to 15 meters using the .srt captions as reference metadata) made inter-annual comparisons difficult. The survey design and workflow presented here did not exist in its final

form prior to data collection. Rather, it developed iteratively over the course of three seasons of field work and surveys of other sites. It was not possible to retroactively employ appropriate data collection procedures, so in some cases shortcomings in the survey data precluded uniform application of the methods described. For instance, the method to convert SRT video captions into GPS reference data for a set of extracted video frames was identified after field work on Lake Seminole had concluded. It was only during subsequent aerial imagery work that this method to automatically georeference orthomosaics created from video frames was identified, and so the orthomosaics for this study had to be manually georeferenced using control points. This form of georeferencing did not allow for reliable assessments of inter-annual changes in vegetation growth, as the layers from different years did not overlap perfectly.

Generating a shoreline mask from DEM-derived contours turned out to not be practicable. It was incorrectly assumed that for the entire reservoir, the water level could be represented by a single elevation contour; however, the elevation of the water surface trended downward by a few meters between the upper reaches of the reservoir and the confluence. This was particularly evident in long, narrow portions of the reservoir such as Spring Creek. Additionally, the existence of riparian vegetation and uneven shoreline topography meant that the elevation contours did not follow the actual shoreline for any appreciable length. It was possible for limited areas to edit and merge several contour lines together to create a shoreline boundary, but manual digitization based on visual inspection of the imagery turned out to be a more reliable and time-efficient approach.

Although it was hypothesized that the lower flying height of UAS compared to manned aircraft or satellite imagery would lessen the impact of atmospheric effects on image quality, the unique operating conditions of low-altitude flight and small image footprint created other sources of

error and inconsistency that need to be addressed. The primary issue is the amount of time needed to cover the survey area given the small image footprint and slow operating velocity (around 40km/hour). While imagery of the entire reservoir could be obtained with a single manned aircraft flight or satellite image, it took at least two full weeks to cover the survey area with a UAS. Changes in phenology and scene illumination from differing weather conditions during this longer time period introduced in-class and between-class spectral variations. These spurious spectral distinctions complicated image segmentation and classification by preventing the application of one classification training set to the entire survey area. Differences in the classified map would therefore be attributable to differences in training area selection rather than actual changes in vegetation coverage, limiting the overall reliability of the classification.

While image segmentation based on RGB spectral signature alone worked reasonably well in many areas, particularly for emergent macrophytes, in many areas there was significant confusion between spectrally-similar classes. In particular, distinguishing between submerged macrophytes and open water, and topped out, senescent vegetation of all types was problematic. Senescent vegetation, either bleached nearly white by the sun, or covered in lyngbya, exhibited a nearly identical appearance. While different growth pattern and other contextual cues enable a human interpreting the image to differentiate between water lily and senescent hydrilla, the image classification algorithms, which relied primarily on spectral signature, did not effectively differentiate between these classes. This could be improved by incorporating bathymetric data and a set of classification rules. For instance, one of the biggest areas of confusion was beds of senescent hydrilla overtopped with lyngbya being misclassified as floating leaf vegetation. These beds were located in deep water, so a classification rule limiting floating leaf to shallower waters (1-2 meters) would eliminate floating leaf from consideration and increase the likelihood of it

being correctly classified as hydrilla. Misclassification between open water and deeply submerged macrophytes were not so much due to spectral similarity as to over-generalization at the segmentation step. This was common in areas of high turbidity and when imagery was collected in cloudy conditions. Deeply-submerged vegetation adjacent to open water would be apparent upon visual interpretation of the imagery, but the segmented image would amalgamate these areas with open water segments. The only method identified to solve this problem was to decrease the minimum segment size to one, the problems with which were discussed in Chapter 3. One possible solution to this problem would be the use of Multiple Resolution Segmentation (MRS), also referred to as multi-scale GEOBIA, where initially a large scale factor would be used to segment the image into general classes such as open water, upland and wetland vegetation. Portions of the image that are not satisfactorily segmented could then be subset and re-segmented using progressively smaller scale factors. This could also increase the classification accuracy of floating leaf vegetation and other, smaller features of interest in the image. Kim et al. (2014) reported a 6% increase in accuracy of multi-scale GEOBIA over single-scale GEOBIA (82% vs. 76%).

Future Directions

A solution to many of the problems presented in this study would be to use a faster UAS with a longer flight time and higher flying height, such as a fixed-wing UAS (i.e., the senseFly eBEE). The ultra-high resolution, multitemporal imaging capabilities of UAS may be in excess of what is needed merely to identify the presence of certain vegetation types, and so increasing flying height would not necessitate outfitting the UAS with a higher-resolution sensor. The larger image footprint from flying higher would make the survey much more efficient with negligible

results on spatial resolution, and could allow the survey to be conducted in as little as one day, limiting atmospheric and phenological sources of spectral variability. Increasing the size of the image footprint would also increase the reliability of the photogrammetric process in areas where open water predominates, since more features would be present in each image. Limiting the variability caused by phenological and atmospheric changes would also allow for more reliable comparison of classification results between time periods. Flying faster and higher could also allow aerial surveys to be conducted at more frequent time intervals. Drawbacks to using a fixed-wing UAS such as the eBEE include greater impacts of ambient wind on the stability of the aircraft and sensor, which can increase image blur. Cost is also a factor, since the price of the eBEE is an order of magnitude greater than the DJI Phantom (Madden et al. 2019). Improving the on-board sensor capability to include near infrared could provide datasets robust enough for researchers to develop a more nuanced understanding of how changes in climate and human activities alter aquatic vegetation growth, and the role of aquatic macrophytes in biogeochemical processes (Tung-Ching and Chou 2015). The DJI Phantom can be equipped with an NIR-capable sensor, such as the MicaSense RedEdge M-Series, as in Lussem et al. (2019), for around \$5,000 USD. This is expected to be necessary in order to reliably differentiate between macrophyte species.

Timing multiple surveys to coincide with different species' most distinctive phenological stage (i.e., during bloom) would yield more precise estimates of intra-annual and inter-annual variations. Monthly aerial surveys during the growing season of smaller, monotypic vegetation stands could be used to calculate growth rates for individual species and assess competition between exotic and native species. Inter-annual surveys could enable precise delineation of surface area coverage and reveal trends in the relative dominance of any particular species

between years, and relate the observed changes to fluctuations to changes in ecological conditions, including air and water temperature, nutrient flows, and precipitation in the watershed (Shivers 2018a). This type of survey methodology could enable the gross primary productivity (GPP) of the entire reservoir to be calculated.

Conclusion

This study dealt primarily with orthomosaic imagery derived from photogrammetrically-produced 3D models, but did not directly utilize the 3D models for analysis purposes. The use of photogrammetric 3D models from UAS imagery for monitoring, analysis, and visualization of results would be a fruitful object for future ecological research in aquatic environments. UAS-generated 3D models, coupled with the emerging technologies of virtual and augmented reality hardware and applications, promise unparalleled opportunities for remotely visualizing, analyzing, and interacting with our world. By loading the 3D models from the Lake Seminole survey into virtual reality headset such as Oculus Rift, researchers could study the same environment at real-world scale in three dimensions, instead of inspecting a 2D image on a screen. The capacity to create a 3D virtual environment from the survey data presented in this study already exists and, in fact, would require only a few more steps to be fully realized. Virtual reality simulations from UAS-derived SfM photogrammetry are becoming more common in video games and entertainment media, but are not yet being implemented in natural resource management initiatives.

Although flaws in the survey design and execution limited this study in terms of being able to classify vegetation uniformly at the species level or compare inter-annual vegetation coverage, the results show the potential for UAS imagery to be a valuable asset in ecological monitoring of

aquatic environments. Improvements in survey design to ensure consistency, and further enumeration of the segmentation and classification workflow could produce highly accurate vegetation maps not just at the species level, but at the individual plant level, thereby opening new opportunities for ecological research. Progressively finer scales of visualization will not only help answer current research questions, but also open up entirely new avenues of inquiry, as epitomized by the ecologist E. O. Wilson's statement that "*a lifetime can be spent in a Magellanic voyage around the trunk of a single tree*".

References

- Aasen, H., E. Honkavaara, A. Lucieer, and P. Zarco-Tejada (2018). “Quantitative Remote Sensing at Ultra-High Resolution with UAV Spectroscopy: A Review of Sensor Technology, Measurement Procedures, and Data Correction Workflows.” *Remote Sensing* 10: 1091. Retrieved from <https://doaj.org/article/67756162969d4c98a80a57d4769b0c3b>
- Adams, C. (2019). “Tinker, Tailor, Soldier, Thief: An Investigation into the Role of Drones in Journalism.” *Digital Journalism* 7(5): 658–677. Retrieved from <https://doi-org.proxy-remote.galib.uga.edu/10.1080/21670811.2018.1533789>
- Antonio, D. (2016). “Drones: New Tools for Natural Risk Mitigation and Disaster Response.” *Current Science* (00113891), 110(6): 958–959. Retrieved from <http://search.ebscohost.com.proxy-remote.galib.uga.edu/login.aspx?direct=true&db=a9h&AN=114007488&site=eds-live>
- Apple, Inc. (2019). iPad Mini - Technical Specification [Online Resource]. Retrieved from https://support.apple.com/kb/sp709?locale=en_US
- ARC (2018a). “Tri-State Water Wars – Background and History.” Atlanta Regional Commission. Retrieved from <https://atlantaregional.org/natural-resources/water-wars/tri-state-water-wars-background-and-history/>

ARC (2018b). "U.S. Supreme Court: Equitable Apportionment." Atlanta Regional Commission. Retrieved from <https://atlantaregional.org/natural-resources/water-wars/u-s-supreme-court-equitable-apportionment/>

Archambault, J., C. Bergeron, G. Cope, R. Richardson, M. Heilman, E. Corey, M. Netherland, and R. Heise (2015). "Sensitivity of Freshwater Molluscs to Hydrilla-Targeting Herbicides: Providing Context for Invasive Aquatic Weed Control in Diverse Ecosystems." *Journal of Freshwater Ecology* 30.3: 335-348. *CAB Abstracts*. Retrieved from http://explore.bl.uk/primo_library/libweb/action/display.do?tabs=detailsTab&gathStatTab=true&ct=display&fn=search&doc=ETOCvdc_100032775279.0x000001&indx=1&recIds=ETOCvdc_100032775279.0x000001

Aulbach-Smith, C., S. De Kozlowski, and L. Dyck (1996). *Aquatic and Wetland Plants of South Carolina*. South Carolina Dept. of Natural Resources in cooperation with the South Carolina Aquatic Plant Management Council. Retrieved from <http://search.ebscohost.com.proxyremote.galib.uga.edu/login.aspx?direct=true&db=cat06564a&AN=uga.9916062073902959&site=eds-live>

Balkcom, G., and D. Morgan (2011). "Effects of Hydrilla Control on Wintering Waterfowl at Lake Seminole, Georgia." *Georgia Journal of Science* 69.2/3: 102. *Advanced Placement Source*.

Ballesteros, R., J. Ortega, D. Hernández, and M. Moreno (2014). “Applications of Georeferenced High-Resolution Images Obtained with Unmanned Aerial Vehicles. Part I: Description of Image Acquisition and Processing.” *Precision Agriculture* 15.6: 579-592. doi: 10.1007/s11119-014-9355-8

Barrientos, C., and M. Allen (2008). “Fish Abundance and Community Composition in Native and Non-Native Plants following Hydrilla Colonisation at Lake Izabal, Guatemala.” *Fisheries Management & Ecology*. 15(2): 99–106. Retrieved from: <https://doi-org.proxy-remote.galib.uga.edu/10.1111/j.1365-2400.2007.00588.x>

Belgiu, M., and L. Drḁgut (2014). “Comparing Supervised and Unsupervised Multiresolution Segmentation Approaches for Extracting Buildings from Very High Resolution Imagery.” *ISPRS Journal of Photogrammetry and Remote Sensing*. 96: 67-75. Retrieved from <https://doi.org/10.1016/j.isprsjprs.2014.07.002>

Blanco, A., W. Roper, and J. Qu (2012). “Spectral Signatures of Hydrilla from a Tank and Field Setting.” *Frontiers of Earth Science* 6.4: 453-460. doi:10.1007/s11707-012-0331-1

Blaschke, T. (2010). “Object Based Image Analysis for Remote Sensing: Review Article.” *ISPRS Journal of Photogrammetry and Remote Sensing* 65: 2-16. doi:10.1016/j.isprsjprs.2009.06.004

Blaschke, T., G. Hay, M. Kelly, S. Lang, P. Hofmann, E. Addink, R. Feitosa, F. van der Meer, H. van der Werff, F. van Coillie, and D. Tiede (2014). “Geographic Object-Based Image Analysis – Towards a New Paradigm.” *ISPRS Journal of Photogrammetry and Remote Sensing* 87: 180–191. Retrieved from <https://doi-org.proxy-remote.galib.uga.edu/10.1016/j.isprsjprs.2013.09.014>

Blaschke, T., S. Lang and G. Hay (Eds.) (2008). *Object-Based Image Analysis: Spatial Concepts for Knowledge-Driven Remote Sensing Applications*. Springer-Verlag, Berlin, 804 p.

Center, T., K. Parys, M. Grodowitz, G. Wheeler, F. Dray, C. O’Brien, S. Johnson, and A. Confrancesco (2013). “Evidence of Establishment of *Bagous hydrillae* (Coleoptera: Curculionidae), a Biological Control Agent of *Hydrilla verticillata* (Hydrocharitales: Hydrocharitaceae) in North America?” *Florida Entomologist* 96.1: 180-186. doi: 10.1653/024.096.0124

Chathuranga, P., D. Dissanayake, N. Priyantha, S. Iqbal, M. Mohamed Iqbal (2014). “Biosorption and Desorption of Lead (II) by *Hydrilla verticillata*.” *Bioremediation Journal* 18.3: 192. doi: 10.1080/10889868.2014.910492

Cho-ying, H., and G. Asner (2009). “Applications of Remote Sensing to Alien Invasive Plant Studies.” *Sensors (14248220)* 9.6: 4869-4889. doi: 10.3390/s90604869

Colomina, I., and P. Molina (2014). “Unmanned Aerial Systems for Photogrammetry and Remote Sensing: A Review.” *ISPRS Journal of Photogrammetry and Remote Sensing* 92: 79-97. Retrieved from <https://doi.org/10.1016/j.isprsjprs.2014.02.013>

Cox, M., R. Wersal, J. Madsen, P. Gerard, M. Tagert (2014). “Assessing the Aquatic Plant Community within the Ross Barnett Reservoir, Mississippi.” *Invasive Plant Science and Management* 7.2: 375-383. doi: 10.1614/IPSM-D-13-00044.1

DJI (2016). Phantom 3 Professional Specs [Online Resource]. Retrieved from <https://www.dji.com/phantom-3-pro/info>

Dodd, S., R. Haynie, S. Williams, and S. Wilde (2016). “Alternate Food-Chain Transfer of the Toxin Linked to Avian Vacuolar Myelinopathy and Implications for the Endangered Florida Snail Kite (*Rostrhamus sociabilis*).” *Journal of Wildlife Diseases* (2): 335. doi: 10.1614/IPSM-D-13-00044.1

Eubanks, M., and D. Morgan (2001). “Lake Seminole Hydrilla Action Plan: Development and Implementation.” Proceedings of the 2001 Georgia Water Resources Conference, April 26 and 27, 2001, Athens, Georgia. Retrieved from <http://hdl.handle.net/1853/44096>

Evans, C., C. Barger, D. Moorhead, and G. Douce (2005). “Invasive Weeds in Georgia.” Georgia Invasive Species Task Force. Retrieved from <http://bugwoodcloud.org/mura/gaeppc/assets/File/flyerfinal.pdf>

FAA (2016). Federal Aviation Administration. Fact Sheet – Small Unmanned Aircraft Regulations (Part 107). Retrieved from https://www.faa.gov/news/fact_sheets/news_story.cfm?newsId=20516

Fassett, N., and E. Ogden (1957). *A Manual of Aquatic Plants* (Vol. [Rev. ed.]). Madison: University of Wisconsin Press. Retrieved from <http://search.ebscohost.com.proxy-remote.galib.uga.edu/login.aspx?direct=true&db=e000xna&AN=332984&site=eds-live>

Fisher, J., W. Kelso, and D. Rutherford (2012). “Macrophyte Mediated Predation on Hydrilla-Dwelling Macroinvertebrates.” *Fundamental and Applied Limnology* 181.1: 25-38. *CAB Abstracts*. doi: 10.1127/1863-9135/2012/0174

Flynn, K., and S. Chapra (2014). “Remote Sensing of Submerged Aquatic Vegetation in a Shallow Non-Turbid River Using an Unmanned Aerial Vehicle.” *Remote Sensing* 6.12: 12815-12836. *Academic Search Complete*. doi: 10.3390/rs61212815

Fox, A., and W. Haller (2000). “Production and Survivorship of the Functional Stolons of Giant Cutgrass, *Zizaniopsis miliacea* (Poaceae).” *American Journal of Botany* 87(6): 811–818. Retrieved from <https://www-jstor-org.proxy-remote.galib.uga.edu/stable/2656888>

Frank, A., and A. Manten (1969). "W. Schermerhorn and His Role in the Development of Photogrammetry." *Photogrammetria* 25(2): 41–60. Retrieved from [https://doi-org.proxy-remote.galib.uga.edu/10.1016/0031-8663\(69\)90007-6](https://doi-org.proxy-remote.galib.uga.edu/10.1016/0031-8663(69)90007-6)

Frick, E., D. Hippe, G. Buell, C. Couch, E. Hopkins, D. Wangsness, and J. Garrett (1998). Water Quality in the Apalachicola-Chattahoochee-Flint River Basin, Georgia, Alabama, and Florida, 1992-95: U.S. Geological Survey Circular 1164. Retrieved from <https://pubs.water.usgs.gov/circ1164>

Fritz, C., K. Doernhoefer, T. Schneider, J. Geist, and N. Oppelt (2017). "Mapping Submerged Aquatic Vegetation Using RapidEye Satellite Data: The Example of Lake Kummerow (Germany)." *Water* 9(7): 510. Retrieved from <https://doi-org.proxy-remote.galib.uga.edu/10.3390/w9070510>

Gao, H., Y. Song, C. Lv, X. Chen, H. Yu, J. Peng, and M. Wang (2015). "The Possible Allelopathic Effect of *Hydrilla verticillata* on Phytoplankton in Nutrient-Rich Water." *Environmental Earth Sciences* 73.9: 5141-5151. *Environment Complete*. doi: 10.1007/s12665-015-4316-8

Green, K. (2017). *Imagery and GIS: Best Practices for Extracting Information from Imagery*. Esri Press.

Hao, J., D. Zhao, H. Zhao, Y. Cai, D. Xu, C. Zhou, X. Leng, and D. Xie (2015). “Density-Dependent Interactions between *Hydrilla verticillata* (L.F.) Royle and Phytoplankton: A Mesocosm Experiment.” *CLEAN: Soil, Air, Water* 43.12: 1623-1632. *Environment Complete*. doi: 10.1002/clen.201300862

Hallerman, T. (2018). “Georgia is Nowhere Near Last Battle in Tri-State Water Wars.” *Atlanta Journal Constitution*. Retrieved from <https://www.ajc.com/news/state--regional-govt-politics/georgia-nowhere-near-last-battle-tri-state-water-wars/qJB83iFrQDCJQV4F5ZPTRJ/>

Hardin, P., V. Lulla, R. Jensen, and J. Jensen (2019). “Small Unmanned Aerial Systems (sUAS) for Environmental Remote Sensing: Challenges and Opportunities Revisited.” *GIScience & Remote Sensing* (2): 309. Retrieved from http://explore.bl.uk/primo_library/libweb/action/display.do?tabs=detailsTab&gathStatTab=true&ct=display&fn=search&doc=ETOCvdc_100075035699.0x000001&indx=1&recIds=ETOCvdc_100075035699.0x000001

Harvey, R., G. Patterson, and J. Pickett (1988). “An Automated Positioning System for Determining Aquatic Macrophyte Distribution.” *Journal of Aquatic Plant Management*. 26: 38-43. *Georef*.

Harwin, S., and A. Lucieer (2012). “Assessing the Accuracy of Georeferenced Point Clouds Produced via Multi-View Stereopsis from Unmanned Aerial Vehicle (UAV) Imagery.” *Remote Sensing* 4: 1573–1599. *Academic Search Complete*. doi: 10.3390/rs4061573

Hassler, S., and F. Baysal-Gurel (2019). “Unmanned Aircraft System (UAS) Technology and Applications in Agriculture.” *Agronomy* 10: 618. Retrieved from <https://doi-org.proxy-remote.galib.uga.edu/10.3390/agronomy9100618>

Hay, G., D. Marceau, P. Dubé, and A. Bouchard (2002). “A Multiscale Framework for Landscape Analysis: Object-Specific Analysis and Upscaling.” *Landscape Ecology* 16: 471-490. Retrieved from <http://search.ebscohost.com.proxy-remote.galib.uga.edu/login.aspx?direct=true&db=edsbl&AN=RN105238022&site=eds-live>

Hay, G., and G. Castilla (2008). “Geographic Object-Based Image Analysis (GEOBIA): A New Name for a New Discipline.” In, Blaschke, T., S. Lang and G.J. Hay (Eds.). *Object-Based Image Analysis: Spatial Concepts for Knowledge-Driven Remote Sensing Applications*. Springer-Verlag, Berlin pp. 91-110.

Husson, E., O. Hagner, and F. Ecke (2014). “Unmanned Aircraft Systems Help to Map Aquatic Vegetation.” *Applied Vegetation Science* 17.3: 567-577. *CAB Abstracts*. Retrieved from http://explore.bl.uk/primo_library/libweb/action/display.do?tabs=detailsTab&gathStatTab=true&ct=display&fn=search&doc=ETOCRN354817273&indx=1&recIds=ETOCRN35481727

Jinning, Z., D. Yu, and X. Xu (2015). “The Phylogeographic Structure of *Hydrilla verticillata* (Hydrocharitaceae) in China and Its Implications for the Biogeographic History of this Worldwide-Distributed Submerged Macrophyte.” *BMC Evolutionary Biology* 15.1: 1-11. *Academic Search Complete*. doi: 10.1186/s12862-015-0381-6

Johnson, K., J. Dotson, W. Pouder, N. Trippel, and R. Eisenhauer (2014). “Effects of Hurricane-Induced Hydrilla Reduction on the Largemouth Bass Fishery at Two Central Florida Lakes.” *Lake and Reservoir Management* 30.3: 217-225. *Science Citation Index*.
Retreived from
http://explore.bl.uk/primo_library/libweb/action/display.do?tabs=detailsTab&gathStatTab=true&ct=display&fn=search&doc=ETOCvdc_100032944026.0x000001&indx=1&recIds=ETOCvdc_100032944026.0x000001

Kaneko, K., and S. Nohara (2014). “Review of Effective Vegetation Mapping Using the UAS (Unmanned Aerial Vehicle) Method.” *Journal of Geographic Information System* 6.6: 733-742. *CAB Abstracts*.

Kim, M., T. Warner, M. Madden, and D. Atkinson (2011). “Multi-scale GEOBIA with Very High Spatial Resolution Digital Aerial Imagery: Scale, Texture and Image Objects.” *International Journal of Remote Sensing*. 32(10): 2825-2850.
doi:10.1080/01431161003745608

Klemas, V. (2015). "Coastal and Environmental Remote Sensing from Unmanned Aerial Vehicles: An Overview." *Journal of Coastal Research* 31.5: 1260-1267. *Science Citation Index*. doi: 10.2112/JCOASTRES-D-15-00005.1

Kumar, A., C. Cooper, C. Remillard, S. Ghosh, A. Haney, F. Braun, Z. Conner, B. Page, K. Boyd, S. Wilde, and D. Mishra (2019). "Spatiotemporal Monitoring of Hydrilla [*Hydrilla verticillata* (L. f.) Royle] to Aid Management Actions." *Weed Technology* 33(3): 518. Retrieved from <http://search.ebscohost.com.proxy-remote.galib.uga.edu/login.aspx?direct=true&db=edb&AN=137099880&site=eds-live>

Lang, S., E. Schöpfer, and T. Langanke (2009). "Combined Object-Based Classification and Manual Interpretation-Synergies for a Quantitative Assessment of Parcels and Biotopes." *Geocarto International* 24(2): 99–114. Retrieved from <https://doi-org.proxy-remote.galib.uga.edu/10.1080/10106040802121093>

Levin, E., K. Vach, and R. Shults (2017). "Development of the New Educational Content 'Small UAS in Civil Engineering Application Scenarios.'" *ISPRS Annals of the Photogrammetry, Remote Sensing and Spatial Information Sciences* 29. Retrieved from <https://doaj.org/article/f15d5f83e7484aa5b51089e2c19c1eb1>

Li, C., B. Wang, C. Ye, and Y. Ba (2014). "The Release of Nitrogen and Phosphorus during the Decomposition Process of Submerged Macrophyte (*Hydrilla verticillata* Royle) with

Different Biomass Levels.” *Ecological Engineering* 70: 268-274. *CAB Abstracts*. doi: 10.1016/j.ecoleng.2014.04.011

Lussem, U., A. Bolten, J. Menne, M. Gnyp, and G. Bareth (2019). “Ultra-High Spatial Resolution UAV-Based Imagery to Predict Biomass in Temperate Grasslands.” *International Archives of the Photogrammetry, Remote Sensing & Spatial Information Sciences, XLII-2/W13*: 443. doi: 10.5194/isprs-archives-XLII-2-W13-443-2019

Maceina, M., and J. Slipke (2004). “The Use of Herbicides to Control Hydrilla and the Effects on Young Largemouth Bass Population Characteristics and Aquatic Vegetation in Lake Seminole, Georgia.” *Journal of Aquatic Plant Management* 42: 5-11. *CAB Abstracts*.

Retrieved from

http://explore.bl.uk/primo_library/libweb/action/display.do?tabs=detailsTab&gathStatTab=true&ct=display&fn=search&doc=ETOCRN153383523&indx=1&recIds=ETOCRN153383523

3

Madden, M. (2004). “Remote Sensing and GIS Methodologies for Vegetation Mapping of Invasive Exotics.” *Weed Technology* 18: 1457-1463.

Madden, M., T. Jordan, S. Bernardes, D. Cotten, N. O’Hare, and A. Pasqua (2015).

“Unmanned Aerial Systems (UAS) and Structure from Motion (SfM) Revolutionize Wetlands Mapping.” In, R. Tiner, M. Lang and V. Klemas (Eds), *Remote Sensing of*

Wetlands: Applications and Advances, CRC Press Taylor & Francis Group, Boca Raton, Florida, 10: 195-222.

Madden, M., T. Jordan, S. Bernardes, C. Goetcheus, K. Olson, and D. Cotton (2019). Small Unmanned Aerial Systems (sUAS) and Structure from Motion (SfM) for Identifying, Documenting and Monitoring Cultural and Natural Resources, In, J.B. Sharma (Ed), *Applications of Small Unmanned Aircraft Systems: Best Practices and Case Studies*. CRC Press Taylor & Francis Group, Boca Raton, Florida. 179-209.

Madsen, J., and C. Owens (1996). "Aquatic Plant Control Research Program (1996)." In *Phenological Studies to Improve Hydrilla Management*." Vol A-96-2. *OAIster*.

Magee, D. (1981). *Freshwater Wetlands: A Guide to Common Indicator Plants of the Northeast*. Amherst: University of Massachusetts Press.

Manuel, K., J. Kirk, D. Barwick, and T. Bowen (2013). "Hydrilla Management in Piedmont Reservoirs Using Herbicides and Triploid Grass Carp: A Case Study." *North American Journal of Fisheries Management* 33.3: 488-492. *CAB Abstracts*.

Mathews, A. (2014). "Object-Based Spatiotemporal Analysis of Vine Canopy Vigor Using an Inexpensive Unmanned Aerial Vehicle Remote Sensing System." *Journal of Applied Remote Sensing* 8. Retrieved from <https://doi-org.proxy-remote.galib.uga.edu/10.1117/1.JRS.8.085199>

Mesas-Carrascosa, F., J. Torres-Sánchez, I. Clavero-Rumbao, A. Garcia-Ferrer, J. Peña, I. Borra-Serrano, and F. López-Granados (2015). “Assessing Optimal Flight Parameters for Generating Accurate Multispectral Orthomosaicks by UAS to Support Site-Specific Crop Management.” *Remote Sensing* 7.10: 12793-12814. *Academic Search Complete*.

Michez, A., H. Piégay, J. Lisein, H. Claessens, and P. Lejeune (2016). “Mapping of Riparian Invasive Species with Supervised Classification of Unmanned Aerial System (UAS) Imagery.” *International Journal of Applied Earth Observation and Geoinformation* 44: 88-94. *Science Citation Index*. doi: 10.1016/j.jag.2015.06.014

Mishra, N., K. Mainali, B. Shrestha, and J. Radenz (2018). “Species-Level Vegetation Mapping in a Himalayan Treeline Ecotone Using Unmanned Aerial System (UAS) Imagery.” *ISPRS International Journal of Geo-Information* 7(11). Retrieved from <https://doi-org.proxy-remote.galib.uga.edu/10.3390/ijgi7110445>

Mora, C., G. Vieira, P. Pina, M. Lousada, and H. Christiansen (2015). “Land Cover Classification Using High-Resolution Aerial Photography in Adventdalen, Svalbard.” *Geografiska Annaler Series A-Physical Geography* 97.3: 473-488. *Science Citation Index*. doi: 10.1111/geoa.12088

McNeal, G. (2014) “Drones and Aerial Surveillance: Considerations for Legislators.”

Brookings Institution. Retrieved from <https://www.brookings.edu/research/drones-and-aerial-surveillance-considerations-for-legislatures/>

Nagid, E., T. Tuten, and K. Johnson (2015). “Effects of Reservoir Drawdowns and the Expansion of Hydrilla Coverage on Year-Class Strength of Largemouth Bass.” *North American Journal of Fisheries Management* 35.1: 54-61. *Science Citation Index*.

Nakada, R., M. Takigawa, T. Ohga, and N. Fujii (2016). “Verification of Potency of Aerial Digital Oblique Cameras for Aerial Photogrammetry in Japan.” *International Archives of the Photogrammetry, Remote Sensing, and Spatial Information Sciences* XLI-B1: 63-68.

Retrieved from <https://doi.org/10.5194/isprs-archives-XLI-B1-63-2016>

NASA DEVELOP (2014). “Developing a Cyanobacteria Detection Tool for Georgia Inland Waters Using NASA LANDSAT-8 OLI Data for Water Quality Protection and Restoration.” NASA DEVELOP National Program, Georgia Node. Retrieved from https://develop.larc.nasa.gov/2014/summer_term/GeorgiaWaterResources.html

Netherland, M., and D. Jones (2015). “Fluridone-Resistant Hydrilla (*Hydrilla verticillata*) is Still Dominant in the Kissimmee Chain of Lakes, FL.” *Invasive Plant Science & Management* 8.2: 212-218. *Environment Complete*. doi: 10.1614/IPSM-D-14-00071.1

Partridge, D. (1996). "Effects of Hydrilla on Water Quality in Lake Seminole, Georgia." Department of Natural Resources, Wildlife Resources Division, Fisheries Management Section. Retrieved from http://dlg.galileo.usg.edu.proxy-remote.galib.uga.edu/id:dlg_ggpd_s-ga-bn200-pg2-bm1-b1996-bh9

Plisson, H., and L. Zotkina (2015). "From 2D to 3D at Macro- and Microscopic Scale in Rock Art Studies." *Digital Applications in Archaeology and Cultural Heritage* 2(2–3), 102–119. Retrieved from <https://doi-org.proxy-remote.galib.uga.edu/10.1016/j.daach.2015.06.002>

Remillard, M., and R. Welch (1992). "GIS Technologies for Aquatic Macrophyte Studies: I. Database Development and Changes in the Aquatic Environment." *Landscape Ecology* 7(3): 151-162.

Remillard, M., and R. Welch (1993). "GIS Technologies for Aquatic Macrophyte Studies: II Modeling Applications." *Landscape Ecology* 8(3): 163-175. *Supplemental Index*.

Remondino, F., M. Spera, E. Nocerino, F. Menna, and F. Nex (2014). "State of the Art in High Density Image Matching." *Photogrammetric Record* 29: 144. Retrieved from <https://doi-org.proxy-remote.galib.uga.edu/10.1111/phor.12063>

Röder, M., S. Hill, and H. Latifi (2017). "Best Practice Tutorial: Technical Handling of the UAV 'DJI 3 Professional' and Processing of the Acquired Data." doi: 10.13140/RG.2.2.36355.91680.

Romero-Oliva, C., V. Contardo-Jara, and S. Pflugmacher (2015). “Antioxidative Response of the Three Macrophytes *Ceratophyllum demersum*, *Egeria densa*, and *Hydrilla verticillata* to a Time Dependent Exposure of Cell-Free Crude Extracts Containing Three Microcystins from Cyanobacterial Blooms of Lake Amatitlán, Guatemala.” *Aquatic Toxicology* [serial online]. 163:130-139. *ScienceDirect*. doi: 10.1016/j.aquatox.2015.04.001

Rotta, L., D. Mishra, E. Alcântara, and N. Imai (2016). “Analyzing the Status of Submerged Aquatic Vegetation Using Novel Optical Parameters.” *International Journal of Remote Sensing* 37(16): 3786-3810. doi:10.1080/01431161.2016.1204027

Salamí, E., and C. Barrado (2014). “UAS Flight Experiments Applied to the Remote Sensing of Vegetated Areas.” *Remote Sensing* 6.11: 11051-11081. *Academic Search Complete*.

Sammons, S., and M. Maceina (2006). “Changes in Diet and Food Consumption of Largemouth Bass following Large-Scale Hydrilla Reduction in Lake Seminole, Georgia.” *Hydrobiologia* 560.1: 109-120. *Food Science Source*. doi: 10.1007/s10750-005-1163-8

Sarma, S., and D. Upen (2014). “Quantitative Analysis of Macrophytes And Physico-Chemical Properties of Water of Two Wetlands of Nalbari District of Assam, India.” *Annals of Biological Research* 5.5: 77-84. *CAB Abstracts*.

Shuchman, R., M. Sayers, and C. Brooks (2013). "Mapping and Monitoring the Extent of Submerged Aquatic Vegetation in the Laurentian Great Lakes with Multi-Scale Satellite Remote Sensing." *Journal of Great Lakes Research* 39(Supplement 1): 78–89. Retrieved from <https://doi-org.proxy-remote.galib.uga.edu/10.1016/j.jglr.2013.05.006>

Singh, A., C. Kumar, and A. Agarwal (2013). "Effect of Lead and Cadmium on Aquatic Plant *Hydrilla verticillata*." *Journal of Environmental Biology* 34.6: 1027-1031. *Environment Complete*.

Shivers, S., S. Golladay, M. Waters, S. Wilde, P. Ashford, and A. Covich (2018a). "Changes in Submerged Aquatic Vegetation (SAV) Coverage Caused by Extended Drought and Flood Pulses." *Lake and Reservoir Management* 34: 218-229. *Taylor & Francis Online*.

Shivers, S., S. Golladay, M. Waters, S. Wilde, and A. Covich (2018b). "Rivers to Reservoirs: Hydrological Drivers Control Reservoir Function by Affecting the Abundance of Submerged and Floating Macrophytes." *Hydrobiologia* 815: 21-35. doi: 10.1007/s10750-018-3532-0

Shivers, S., S. Opsahl, and A. Covich (2016). "Microbial Bioavailability of Dissolved Organic Carbon from Leachates of Freshwater Autotrophs." *Aquatic Microbial Ecology*, 76: 233-241. Retrieved from <http://search.ebscohost.com.proxy-remote.galib.uga.edu/login.aspx?direct=true&db=edsbl&AN=RN605261564&site=eds-live>

Smith, M., J. Carrivick, and D. Quincey (2016). "Structure from Motion Photogrammetry in Physical Geography." *Progress in Physical Geography* 40(2), 247.

doi: 10.1177/0309133315615805

Sousa, W. (2011). "*Hydrilla verticillata* (Hydrocharitaceae), a Recent Invader Threatening Brazil's Freshwater Environments: A Review of the Extent of the Problem." *Hydrobiologia* 669.1: 1-20. *Food Science Source*.

Spence, C., and S. Mengistu (2016). "Deployment of an Unmanned Aerial System to Assist in Mapping an Intermittent Stream." *Hydrological Processes* 30.3: 493-500. *Environment Complete*. doi: 10.1002/hyp.10597

Srivastava, S., S. Sounderajan, A. Udas, and P. Suprasanna (2014). "Effect of Combinations of Aquatic Plants (*Hydrilla*, *Ceratophyllum*, *Eichhornia*, *Lemna* and *Wolffia*) on Arsenic Removal in Field Conditions." *Ecological Engineering* 73: 297-301. *Science Citation Index*.

Srivastava, S., and K. Bhainsa (2016). "Evaluation of Uranium Removal by *Hydrilla verticillata* (L.F.) Royle from Low Level Nuclear Waste under Laboratory Conditions." *Journal of Environmental Management* 167: 124-129. *Environment Complete*.

Tamminga, A., C. Hugenholtz, B. Eaton, and M. Lapointe (2015). "Hyperspatial Remote Sensing of Channel Reach Morphology and Hydraulic Fish Habitat Using an Unmanned

Aerial Vehicle (UAV): A First Assessment in the Context of River Research and Management.” *River Research and Applications* 31.3: 379-391. *CAB Abstracts*.

Tung-Ching, S., and H. Chou (2015). “Application of Multispectral Sensors Carried on Unmanned Aerial Vehicle (UAV) to Trophic State Mapping of Small Reservoirs: A Case Study of Tain-Pu Reservoir in Kinmen, Taiwan.” *Remote Sensing* 7: 10078-10097.
doi:10.3390/rs70810078

Umetsu, C., H. Evangelista, and S. Thomaz (2012). “Colonization, Regeneration Potential and Growth Rates of Fragments of the Exotic Aquatic Macrophyte *Hydrilla verticillata*.” *Aquatic Biology* 16.2: 197-202. *CAB Abstracts*.

Underwood, E., M. Mulitsch, J. Greenberg, M. Whiting, S. Ustin, and S. Kefauver (2006). “Mapping Invasive Aquatic Vegetation in the Sacramento-San Joaquin Delta Using Hyperspectral Imagery.” *Environmental Monitoring & Assessment* 121.1-3: 47-64. *Food Science Source*.

USGS (2017). “Unmanned Aircraft Systems Data Post-Processing.” United States Geological Survey. UAS Federal Users Workshop. Retrieved from
<https://uas.usgs.gov/pdf/MetashapeProcessingDSLRLMar2017.pdf>

Waagen, J. (2019). “New Technology and Archaeological Practice: Improving the Primary Archaeological Recording Process in Excavation by Means of UAS Photogrammetry.”

Journal of Archaeological Science 101: 11–20. Retrieved from <https://doi-org.proxy-remote.galib.uga.edu/10.1016/j.jas.2018.10.011>

Wang, S., X. Jin, H. Zhao, X. Zhou, and F. Wu (2007). “Effects of *Hydrilla verticillata* on Phosphorus Retention and Release in Sediments.” *Water, Air & Soil Pollution* 181.1-4: 329-339. *Food Science Source*.

Waters, M., S. Golladay, C. Patrick, J. Smoak, and S. Shivers (2015). “The Potential Effects of River Regulation and Watershed Land Use on Sediment Characteristics and Lake Primary Producers in a Large Reservoir.” *Hydrobiologia* 749.1: 15-30. *Food Science Source*.

Westoby, M., J. Brasington, N. Glasser, M. Hambrey, and J. Reynolds (2012). “Structure-from-Motion Photogrammetry: A Low-Cost, Effective Tool for Geoscience Applications.” *Geomorphology* 179: 300-314.

Retrieved from <https://doi.org/10.1016/j.geomorph.2012.08.021>

Welch, R., M. Remillard, and R. Slack (1988). “Remote Sensing and Geographic Information System Techniques for Aquatic Resource Evaluation.” *Photogrammetric Engineering and Remote Sensing* 54(2): 177-185.

Wang, S., Y. Wang, Q. Hu., J. Li, and M. Ai. (2019). “Unmanned Aerial Vehicle and Structure-from-Motion Photogrammetry for Three-Dimensional Documentation and Digital

Rubbing of the Zuo River Valley Rock Paintings.” *Archeological Prospection* 26(3): 265–279. <https://doi-org.proxy-remote.galib.uga.edu/10.1002/arp.1739>

Wang, Y., M. Traber, B. Milstead, and S. Stevens (2007). “Terrestrial and Submerged Aquatic Vegetation Mapping in Fire Island National Seashore Using High Spatial Resolution Remote Sensing Data.” *Marine Geodesy* 30.1/2: 77-95. *Science & Technology Collection*.

Whiteside, T., and R. Bartolo (2015). “Mapping Aquatic Vegetation in a Tropical Wetland Using High Spatial Resolution Multispectral Satellite Imagery.” *Remote Sensing* 7: 11664-11694.

Zhang, C., D. Selch, and H. Cooper (2016). “A Framework to Combine Three Remotely Sensed Data Sources for Vegetation Mapping in the Central Florida Everglades.” *Wetlands* 36.2: 201-213. *CAB Abstracts*.

Zhang, T., M. He, A. Wu, and L. Nie (2012). “Inhibitory Effects and Mechanisms of *Hydrilla verticillata* (Linn.F.) Royle Extracts on Freshwater Algae.” *Bulletin of Environmental Contamination & Toxicology* 88.3: 477-481. *Food Science Source*.

Zhang, X., X. Liu, and Q. Ding (2013). “Morphological Responses to Water-Level Fluctuations of Two Submerged Macrophytes, *Myriophyllum spicatum* and *Hydrilla verticillata*.” *Journal of Plant Ecology* 6.1: 64-70. *CAB Abstracts*.